Carbon Neutrality

REVIEW

Open Access

# Research progresses in O3-type Ni/Fe/Mn based layered cathode materials for sodium ion batteries

Shengyu Zhao[1], Qinhao Shi[1], Wuliang Feng[1], Yang Liu[1], Xinxin Yang[2], Xingli Zou[2], Xionggang Lu[2] and Yufeng Zhao[1*]

**Abstract**

Sodium ion batteries (SIBs) have attracted great interest as candidates in stationary energy storage systems relying on low cost, high abundance and outstanding electrochemical properties. The foremost challenge in advanced NIBs lies in developing high-performance and low-cost electrode materials. To accelerate the commercialization of sodium ion batteries, various types of materials are being developed to meet the increasing energy demand. O3-type layered oxide cathode materials show great potential for commercial applications due to their high reversible capacity, moderate operating voltage and easy synthesis, while allowing direct matching of the negative electrode to assemble a full battery. Here, representative progress for Ni/Fe/Mn based O3-type cathode materials have been summarized, and existing problems, challenges and solutions are presented. In addition, the effects of irreversible phase transitions, air stability, structural distortion and ion migration on electrochemical performance are systematically discussed. We hope to provide new design ideas or solutions to advance the commercialization of sodium ion batteries.

**Keywords** Sodium ion batteries, O3-type cathode materials, Cyclic performance

## 1 Introduction

Since the commercialization of lithium-ion batteries by Sony in 1991, they are now widely developed and utilized as energy sources of mobile electronic devices, electric vehicles and hybrid electric vehicles, relying on their high energy density, long cycle life and good theoretical safety. With the rise of the EV and HEV markets, the demand for lithium has increased dramatically, while the uneven distribution and limited reserves of lithium resources in the earth's crust have further triggered the fluctuating prices. Compared with lithium, sodium with high abundance is widely distributed in the earth's crust and sea, and have similar intercalation chemistry [1–5], which demonstrates great potential for application in stationary energy storage systems [6, 7].

Today, research on sodium-ion batteries (NIBs) is growing every year, and their operating principle (Fig. 1a) is similar to lithium-ion batteries. The cathode material plays a vital role in reversible capacity, energy density and lifespan of sodium ion batteries. A broad range of compounds, including layered oxides [8–13], polyanion compounds [14–17], Prussian blue analogues [18–20], have been studied as potential candidates. Among them, layered oxide cathode materials are one of the most promising cathode materials for commercial application due to their appropriate operating voltage, high reversible capacity and facile synthesis [21]. Layer oxide cathode materials ($Na_xTMO_2$) are mainly divided into P2-type and O3-type cathode (Fig. 1b), the letters "P"

*Correspondence:
Yufeng Zhao
yufengzhao@shu.edu.cn
[1] Institute for Sustainable Energy & College of Sciences, Shanghai University, Shanghai 200444, China
[2] State Key Laboratory of Advanced Special Steel and Shanghai Key Laboratory of Advanced Ferrometallurgy and School of Materials Science and Engineering, Shanghai University, Shanghai 200444, China

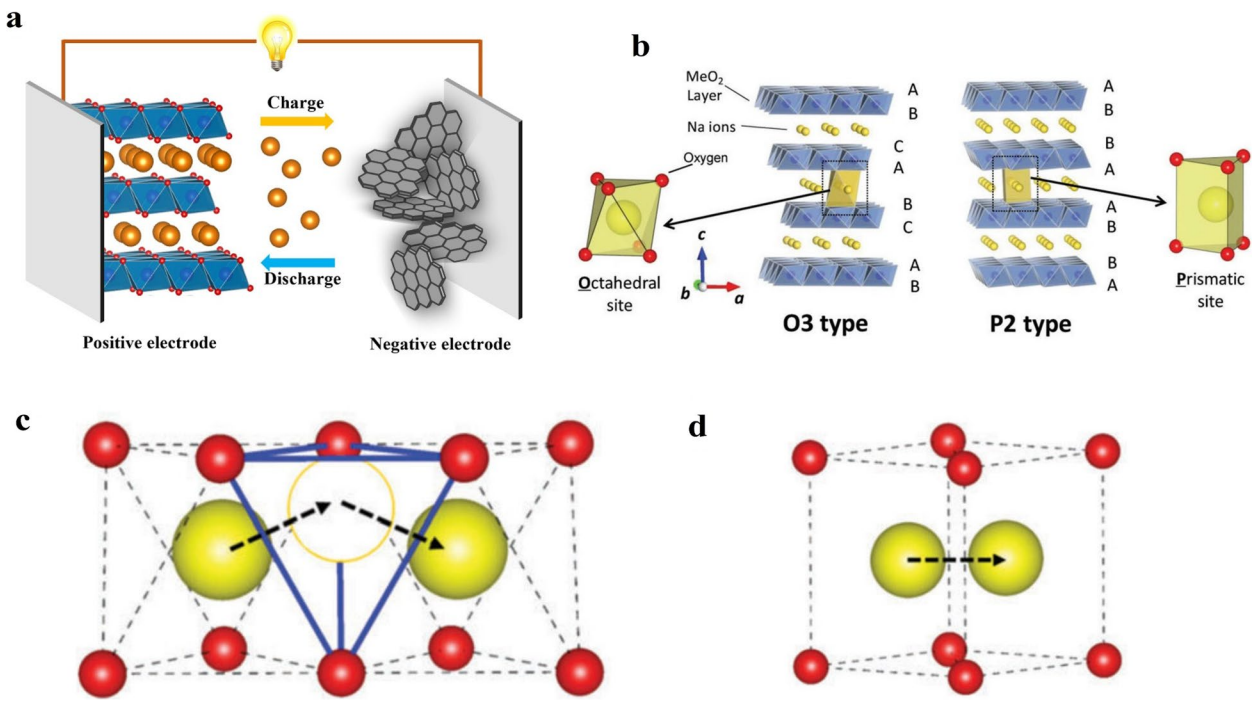


**Fig. 1** **a** Working principles diagram of sodium ion batteries. **b** Schematic illustrations of crystal structures of O3 and P2 type $Na_xTMO_2$. Reproduced with permission [46]. Copyright 2014, American Chemical Society. **c** The indirect Na-ion diffusion path with the intermediate tetrahedron site in O-type frameworks. **d** The direct Na-ion diffusion path without the intermediate site in P-type frameworks. The red and yellow balls represent oxygen ions and sodium ions, respectively. Reproduced with permission [47]. Copyright 2016, Royal Society of Chemistry

and "O" represent the trigonal prismatic coordination environment and octahedral coordination environment of sodium ion, respectively; The number "2" and "3" refer to the number of oxygen stacking layers in one unit cell [22]. In general, O3-type cathode materials have sufficient Na content (x ~ 0.9–1.0) and deliver higher reversible specific capacity, which can be directly matched with anode materials to assemble full cells according to the initial coulombic efficiency (ICE) and reversible capacity of the materials. It is worth pointing out that the widely applied cathode materials of lithium ion batteries such as $LiCoO_2$ and $LiNi_xCo_yMn_zO_2$, are O3 type materials, if the O3 type cathode materials of SIBs can achieve the application, it will be able to achieve rapid large-scale production with the previous process for lithium ion battery. In contrast, P2-type materials are deficient in sodium content (x ~ 0.6–0.8), generally have low capacity with abnormal initial coulombic efficiency, and may require the additional sodium to achieve full-cell assembly. Therefore, O3-type materials are the most promising cathode materials for large-scale commercial applications [23]. In Table 1, the electrochemical performance of recent reported O3-type layered cathode materials for SIBs are presented. It is worth pointing out that O3-type materials require higher migration energy barriers due to the sodium ion migration through intermediate tetrahedral site between two adjacent octahedral sites (Fig. 1c) [21], compared to P2-type materials that can migrate directly between two adjacent trigonal prismatic sites (Fig. 1d). Thus, rate performance of O3-type materials is slightly lower than that of P2-type materials, which can be improved by reasonable adjustment of the crystal structure [24, 25]. The Chinese HiNa has already achieved small scale manufacture of 18,650 cylindrical cells based on Cu-based O3-type material as cathode, with a gravimetric energy density of 135 Wh $kg^{-1}$ and excellent high and low temperature performance [6, 26]. Almost the same time, Ma's group prepared 1 Ah soft-packed sodium-ion battery based on Ni–Fe-Mn based O3 cathode in 2016 [27] and they further achieved a capacity retention of 92.2% after 1000 cycles via using FEC-PST-DTD (FPD) as electrolyte additives [28].

O3-type cathode materials demonstrate great advantages in commercialization, but still face some inherent challenges. On the one hand, with the continuous extraction of Na, the O3-type cathode materials undergo a suite of complex multilevel phase transition involving different stacking sequences of the oxide layers [29, 30]. For instance, the representative O3-type cathode material $NaNi_{0.5}Mn_{0.5}O_2$, the phase transition in charge process in the voltage range of 2.2–4.5 V is corresponding to O3-O'3-P3-P'3-P3" [31, 32]. It should be noted that

**Table 1** Summary of the electrochemical performance of recent reported O3-type layered cathode materials for SIBs

| Materials | Voltage windows(V) | Reversible capacity(mAh $g^{-1}$) | Capacity retention | Ref |
|---|---|---|---|---|
| $NaNi_{0.45}Cu_{0.05}Mn_{0.4}Ti_{0.1}O_2$ | 2–4 | 124 | 70.2% (500 cycles at 1 C) | [11] |
| $NaFeO_2$ | 2.5–3.4 | 80 | 75% (30 cycles at 0.1 C) | [48] |
| $Na_4FeRuO_6$ | 2–4 | 120 | 80% (100 cycles at 2 C) | [49] |
| $NaFeO_2$@C | 2–3.4 | 89.6 | 83.7% (100 cycles at 0.1 C) | [50] |
| $NaMnO_2$ | 2–3.8 | 185 | 71.4% (20 cycles at 0.1 C) | [51] |
| $NaMn_{0.6}Al_{0.4}O_2$ | 1–4 | 160 | 81% (100 cycles at 500 mA $g^{-1}$) | [52] |
| $Na_{1.2}Mn_{0.4}Ir_{0.4}O_2$ | 1.5–4.4 | 179 | 60% (50 cycles at 0.5 C) | [53] |
| $Na[Li_{0.05}Mn_{0.50}Ni_{0.30}Cu_{0.1}0Mg_{0.05}]O_2$ | 2–4 | 172 | 70.4% (1000 cycles at 20 C) | [54] |
| $NaNiO_2$ | 1.25–3.75 | 123 | 94.3% (20 cycles at 0.1 C) | [55] |
| $Na_{0.8}Ni_{0.6}Sb_{0.4}O_2$ | 2–4.3 | 106 | 78% (100 cycles at 1 C) | [56] |
| $Na_{0.7}Ni_{0.35}Sn_{0.65}O_2$ | 2–4 | 64 | 80% (100 cycles at 0.1 C) | [57] |
| $NaTi_{0.5}Ni_{0.5}O_2$ | 2–4 | 102 | 75% (300 cycles at 1 C) | [58] |
| $Na_{0.8}Ni_{0.3}Co_{0.1}Ti_{0.6}O_2$ | 2–4 | 92 | 98% (1000 cycles at 5 C) | [59] |
| $Na_{0.9}Ni_{0.3}Co_{0.15}Mn_{0.05}Ti_{0.5}O_2$ | 2–4 | 112.7 | 81.6% (1000 cycles at 100 C) | [60] |
| $Na_3Ni_2RuO_6$ | 2–3.8 | 130 | 81% (1000 cycles at 1 C) | [61] |
| $Na_3Ni_2SbO_6$ | 2–4 | 120 | 70% (500 cycles at 2 C) | [62] |
| $NaNi_{0.5}Mn_{0.2}Ti_{0.3}O_2$ | 2–4 | 135 | 85% (200 cycles at 5C) | [63] |
| $NaNi_{0.47}Zn_{0.03}Mn_{0.5}O_2$ | 2–4 | 113 | 80% (150 cycles at 0.5C) | [64] |
| $NaNi_{0.5}Mn_{0.1}Sn_{0.4}O_2$ | 2–4.2 | 91 | 85% (200 cycles at 0.1 C) | [65] |
| $MgO\text{-}NaNi_{0.5}Mn_{0.5}O_2$ | 2–4.2 | 167 | 75% (100 cycles at 0.5 C) | [66] |
| $NaFe_{0.2}Ni_{0.4}Mn_{0.4}O_2$ | 2–4 | 131 | 96.4% (30 cycles at 0.05 C) | [67] |
| $NaFe_{0.3}Ni_{0.35}Mn_{0.35}O_2$ | 2–4 | 130.3 | 80% (100 cycles at 1 C) | [68] |
| $NaNi_{0.4}Fe_{0.2}Mn_{0.2}Ti_{0.2}O_2$ | 2–4.2 | 145 | 84% (200 cycles at 0.1 C) | [69] |
| $Na_{0.85}Li_{0.1}Ni_{0.175}Mn_{0.525}Fe_{0.2}O_2$ | 2–4.5 | 160 | 88% (100 cycles at 1 C) | [70] |
| $NaNi_{1/3}Fe_{1/3}Mn1/3O_{1.99}F_{0.01}$ | 2–4 | 122 | 85% (70 cycles at 1 C) | [71] |
| $NaNi_{0.25}Mg_{0.05}Cu_{0.1}Fe_{0.2}Mn_{0.2}Ti_{0.1}Sn_{0.}1O_2$ | 2–4 | 130.8 | 75% (500 cycles at 1 C) | [72] |
| $Na_{0.94}Ni_{0.29}Cu_{0.1}Fe_{0.16}Mn_{0.3}Ti_{0.15}O_2$ | 2–4 | 122 | 79% (300 cycles at 0.5 C) | [73] |
| $Na_2SiO_3$@$NaNi_{1/3}Fe_{1/3}Mn_{1/3}O_2$ | 1.5–4.2 | 134 | 83.3% (200 cycles at 0.5 C) | [74] |
| $ZrO_2$@$NaNi_{1/3}Fe_{1/3}Mn_{1/3}O_2$ | 1.5–4.3 | 152.4 | 81.9% (100 cycles at 1 C) | [75] |
| $Na_{7/9}Ni_{2/9}Mn_{4/9}Fe_{1/9}Mg_{1/9}Li_{1/9}O_2$ | 2.0–4.4 | 170.5 | 71.8% (500 cycles at 5 C) | [76] |

different stacking sequences have widely varying cell parameters, and multi-phase transitions can bring about large volume expansion and internal stresses, leading to the generation of microcracks within the bulk along with continuous electrolyte infiltration and corrosion, further resulting in poor mechanical integrity and capacity degradation [12]. Meanwhile, it needs extra energy barrier for phase boundary movement, leading poor rate capability [21]. On the other hand, the advantage of sodium ion batteries is low cost, so the preferential elements choice for cathode materials should be low cost, high abundance and easy access, such as Fe and Mn. However, Fe will inevitably migrate from the transition metal layer to the sodium layer during the charge–discharge process, which will impede the sodium ion transport and lead to capacity degradation [33, 34]. $Mn^{3+}$ has a strong Jahn–Teller effects, which will cause distortion of the crystal structure and further aggravate the irreversible phase transition [35, 36]. Therefore, the components and valence states of the elements in the O3-type material need to be regulated reasonably in the application. It is worth mentioning that Fe–Mn based O3-type cathode usually have poor cyclic performance and large voltage hysteresis along with a series of impurity phase [37–40]. A large number of articles have pointed out that a small quantity of Ni can greatly improve these disadvantages [41–44]. In addition, poor air stability also limits the commercialization of O3-type cathode materials, which will increase production, transportation and storage costs. O3-type cathode materials are prone to spontaneous exchange of $Na^+$ and $H^+$ in ambient air, resulting in loss of bulk Na and insertion of water in the bulk [43, 45]; Residual Na

species on the particle surface will react with water and $CO_2$ in ambient air to form sodium carbonate, sodium hydroxide etc., which are insulative to sodium ion transport, and excessive surface residual alkali will make the slurry gelation [46].

Currently, the modifications of O3-type cathode materials mainly include ion doping, surface modification and composite structure construction. The ion doping can well suppress the multilevel phase transition and regulate the working voltage; the surface modification can effectively protect the material from electrolyte corrosion and reduce the dissolution of transition metal ions; the composite structure construction can fully utilize the advantages of multiple phases and synergistically improve the comprehensive performance of the cathode material. A great deal of effort has been made to obtain outstanding electrochemical properties.

This review thoroughly summarized recent research progress in modifications of O3-type $Na_xNi_yFe_zMn_{1-y-z}O_2$ layered transition metal oxides, focusing especially on three challenges of irreversible phase transitions, migration of transition metal ions and Jahn–Teller effect, and poor air stability. Meanwhile, a detailed and comprehensive understanding of the intrinsic working mechanisms, structural evolution, and sodium ion storage electrochemistry is discussed. The structure-composition-performance relationship is also revealed. It will provide some inspiration for researchers to carry out studies for commercial application of O3-type cathode materials.

### 1.1 O3-type layered structure

#### *1.1.1 O3-type $Na_xFeO_2$*

Fe-based cathode materials show great potential for the battery applications due to low cost, high abundance in the Earth's crust and nontoxic feature. α-$NaFeO_2$ is an representative O3-type layer cathode, it delivers a reversible capacity of 80 mAh $g^{-1}$ (0.33 mol Na extraction/insertion) along with a flat discharge platform about 3.3 V in the voltage range of 2.5–3.4 V [48], which is similar to that of isostructural $LiCoO_2$ [34]. The electrode performance shows high relevance with cut-off voltage. When the cut-off voltage is surpassed to 3.5 V, the reversibility gradually decreases and polarization drastically increases. The α-$NaFeO_2$ become almost completely inactive when about 0.7 mol Na is extracted. Komaba and co-workers [48] believed that the poor reversibility is resulting from irreversible structural transition and iron ion migration, thus hindering the $Na^+$ re-insertion. Later, chen et al. [77] directly observed iron ion migration to Na layer at the atomic scale and presented the Fe migration from the $O_{Fe}$ to $T_{Na}$ (tetrahedron site in the Na layer) is energetically favorable, which is also verified by DFT calculations (Fig. 2a, b). Recently, Chung and co-workers [78] investigated comprehensively the irreversible phase transition process when more than 0.5 Na is extracted in α-$NaFeO_2$ (Fig. 2c). It is demonstrated that formation of $Fe_3O_4$ in the surface blocks Na insertion into the structure accompanied with oxygen release. More recently, Johnsonand co-workers [79] found that more than 20% of $Fe^{4+}$ have spontaneous tendency to reduce back to $Fe^{3+}$ in a charged state, accompanied by electrolyte decomposition, which is evidenced by exsitu Mössbauer spectroscopy (Fig. 2d). This self-discharge behavior can trigger rapid performance degradation and increase storage cost. Meanwhile, they also presented that desodiation process of α-$NaFeO_2$ is accompanied by coherently nucleated O"3-$Na_{1-x}FO$ and m-$Na_{1-x}FO$ phases in 2.0–3.6 V, rather than to form P3 phase via layer gliding, which is common for most O3-type cathode, such as $NaCrO_2$, $NaCoO_2$ and $NaNi_{0.5}Mn_{0.5}O_2$. The unique phase transition process may ascribe that tetrahedral $Fe^{3+}$ in Na layer resist layer glide and lead to nonuniform extraction of sodium (Fig. 2e).

It is known that solvothermal method can make reactants more uniform in the solution, compared with the common solid state method. Specially, in the synthetic process of $NaFeO_2$, reactive $Na_2O_2$ was usually used as sodium source rather than $Na_2CO_3$ owing to the latter usually easily to form tiny electrochemically inactive β-$NaFeO_2$ [80]. Meanwhile, $Na_2O_2$ is highly sensitive to $H_2O$ and $CO_2$ in ambient air. Thus, it increases difficulty in preparation. Tabuchi [81, 82] et al. prepared high-crystallinity α-$NaFeO_2$ via solvothermal method without $Na_2O_2$, it delivers improved cyclic performance compared to the solid state method. Xia [50] came up with a carbon-coated single crystal O3-$NaFeO_2$ nanoflakes by facile solvothermal route with subsequent carbon-coated (Fig. 3a), which exhibits a high capacity of 89.6 mAh $g^{-1}$ in the voltage range of 2.0–3.4 V and capacity retention of 87.3% after 100 cycles at 0.1C. In addition, carbon coated $NaFeO_2$//hard carbon full cell also presented good cyclic performance with 81.9% capacity retention after 100 cycles.

Thermal stability and air stability are key component for future commercial applications, which is closely relevant to safety and storage performance. Nishida and co-workers [83] compared thermal properties of α-$NaFeO_2$ and $LiCoO_2$ counterparts by DSC measurements. The results indicated that fully-charged α-$NaFeO_2$ presents better thermal stability in the electrolyte than $LiCoO_2$ counterparts with higher exothermic onset temperature and less heat generation. Of note is that α-$NaFeO_2$ have hygroscopic character and $Na^+$ have spontaneous tendency to diffuse to the surface [48], leading to formation of electrochemically inactive phase, such as NaOH, $Na_2CO_3$. It drastically

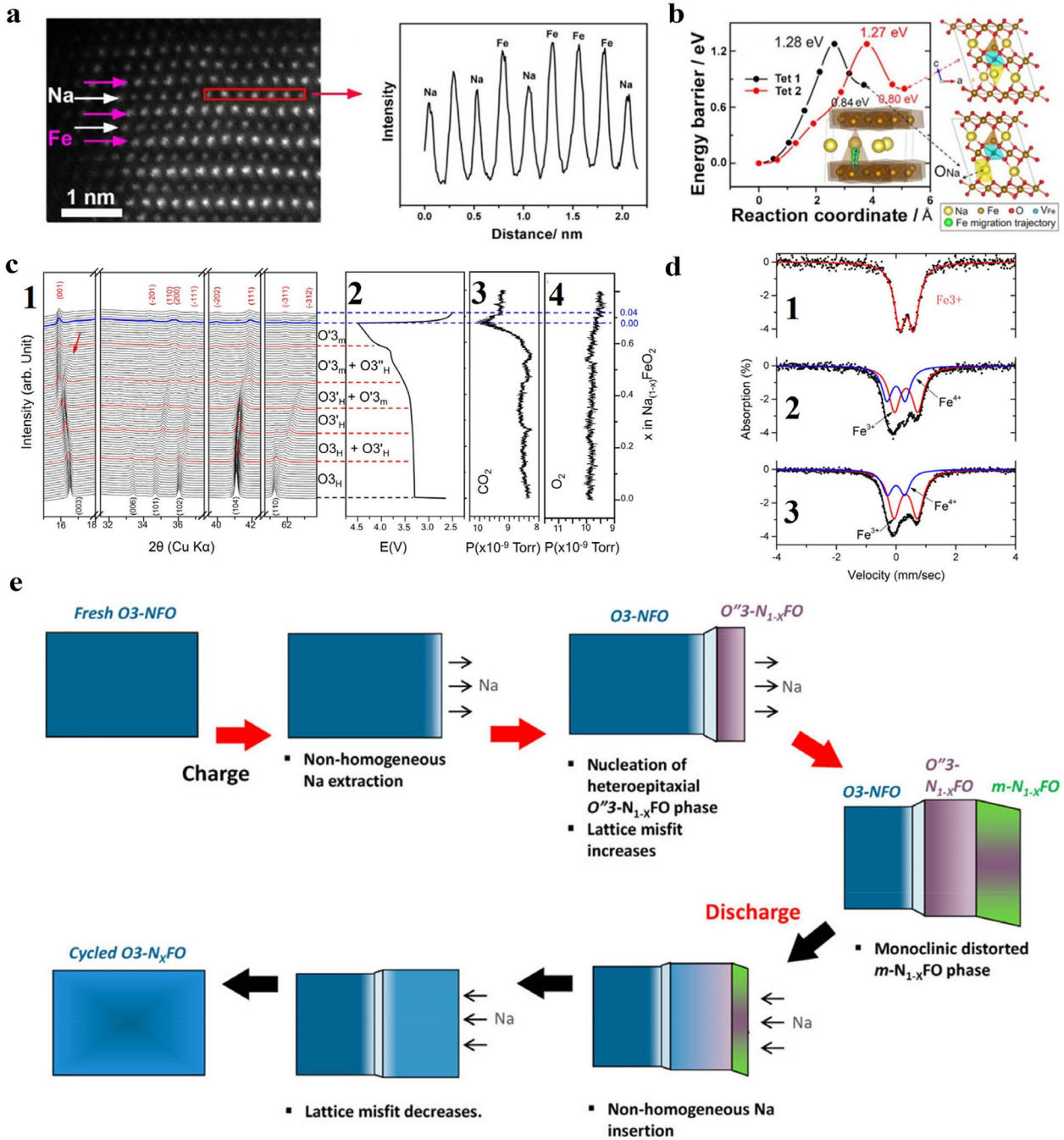


**Fig. 2** **a** The HAADF images of $NaFeO_2$ at the fully charged state and the corresponding line profile acquired from the red rectangular region. **b** Pathways for the direct Fe migration from the $O_{Fe}$ to the $T_{Na}$ sites in $Na_{0.33}FeO_2$. The yellow, brown, red, blue and green balls in the structural schematic are for Na, Fe, O, $V_{Fe}$ and the Fe migration trajectory, respectively. Reproduced with permission [77]. Copyright 2018, Elsevier B.V. **c** $c_1$ In-situ synchrotron X-ray diffraction patterns of $Na_{1-x}FeO_2$ showing the characteristic hkl peak in different phases. $c_2$ In-situ galvanostatic charge and discharge profiles at a rate of 0.05 C with a cutoff voltage of 4.5 V. The arrow indicates broadening of the (003) peak of $O3'_H$. $c_3$ and $c_4$ $CO_2$ and $O_2$ gas evolution from $NaFeO_2$ during sodium extraction and insertion. Reproduced with permission [78]. Copyright 2019, American Chemical Society. **d** Ex situ Mössbauer spectra for $NaFeO_2$ electrodes $a_1$ in the pristine state, $a_2$ charged to 0.46 SOC, and $a_3$ stored for 2 days under open circuit conditions after being charged to 0.5 SOC. **e** Schematic illustration of the proposed coherent phase evolution during electrochemical cycling of α-$NaFeO_2$. Reproduced with permission [79]. Copyright 2015, American Chemical Society

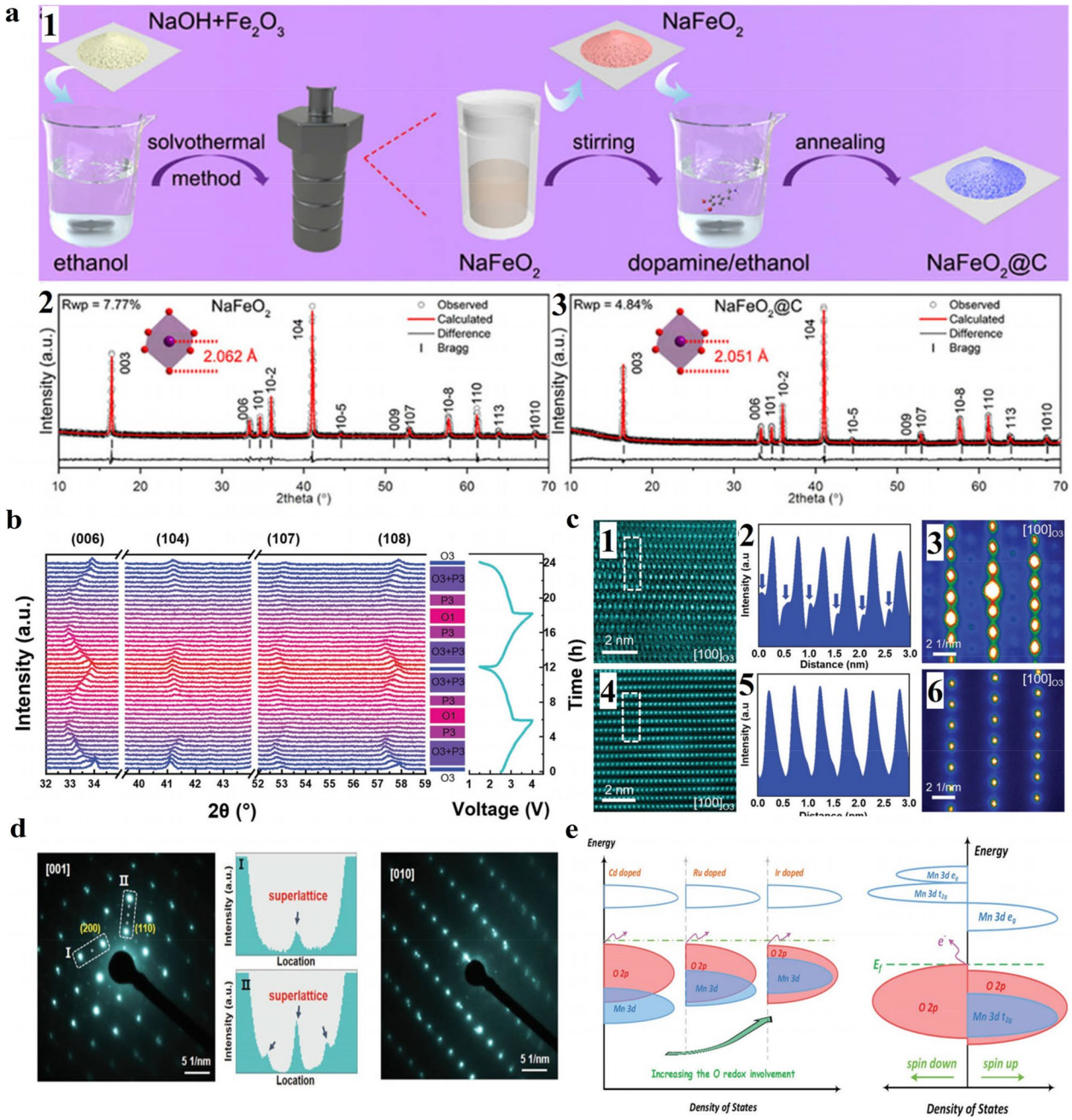


**Fig. 3** **a** $a_1$ Schematic illustration of the synthesis procedure of the $NaFeO_2$ and $NaFeO_2$@C samples. Rietveld-refined XRD patterns of the $NaFeO_2$ $a_2$ and $NaFeO_2$@C $a_3$ samples, respectively. Reproduced with permission [50]. Copyright 2021, Elsevier B.V. **b** In situ XRD patterns of the NFRO cathode under a current rate of 0.25C at voltage range between 1.5 and 4 V. **c** Atomic STEM-HAADF images of $c_1$ NFO and $c_4$ NFRO samples charging to 4 V; $c_2$ Line-profile of selected area by dash line in $c_1$, the blue arrow in $c_2$ indicates the migration of Fe ions into Na layers; $c_5$ Line-profile of selected area by dash line in $c_4$; Nanobeam electron diffraction patterns of $c_3$ NFO and $c_6$ NFRO samples charging to 4 V. Reproduced with permission [49]. Copyright 2019, Wiley–VCH. **d** SAED patterns of sample viewed along the [1] axis and [10] axis, respectively, (I and II are the corresponding line-profiles of the marked regions in SAED pattern). Reproduced with permission [52]. Copyright 2021, Wiley–VCH. **e** Schematic illustration of the DOS for chosen potential doping species and Ir-doped $Na_{1.2}Mn_{0.4}Ir_{0.4}O_2$. The O-2p band and Mn 3d band are depicted in red and blue, respectively. The Cd Ru and Ir doped Mn-based Na-rich system has a tendency for increasing O redox improvement as the Mn 3d band increases from the deep part, which refers to a suppression of $O_2$ release. Reproduced with permission [53]. Copyright 2019, Wiley–VCH

impedes their practical viability (gelation of the slurry) and decrease the electrochemical performance. Thus, it is essential to incorporate proper ion or surface coating to realize improved air stability. Nevertheless, the focus on air stability for $NaFeO_2$ is still few.

Although α-$NaFeO_2$ have been widely developed depending on the economic efficiency, high abundance, thermal stability, and high voltage platform, the cyclic performance is still unsatisfactory for potential application, which is closely relevant to Fe migration and irreversible phase transformation. Zhou and co-workers [49] reported an Ru-substitution $Na_4FeRuO_6$ cathode which exhibited a high reversible capacity of 120 mAh $g^{-1}$ and superior capacity retention of 80% over 100 cycles based on reversible O3-P3-O1 phase transformation (Fig. 3b). In contrast, $NaFeO_2$ severely decay to about 10 mAh $g^{-1}$ after several cycles and presents an irreversible phase of O'3 and O"3. The larger size of $Ru^{4+}$ effectively suppress the irreversible migration of Fe ions, which is clearly characterized on an atomic scale by HAADF-STEM (Fig. 3c). Then, the less Fe ion migration maintain the well structure integrality and decrease the local lattice strain, thus particle cracks was remarkably reduced. For all we know that particle crack is one of the main reasons for performance deterioration. Once the mass of cracks generates, the $Na^+$ transport channel will be blocked and layer structure may be destroyed during long term cycling, leading to the battery failure eventually [12, 84]. Thus, it is vital to reduce the micro-crack by proper strategy. In addition, Mg introduction to α-$NaFeO_2$ also was demonstrated to greatly reduces migration of Fe ions and increases capacity and cycling stability [85]. Guo et al. prepared a new cathode $NaFe_{0.45}Co_{0.5}Mg_{0.05}O_2$ based on the synergetic effect of multi-metal ions, in which $Fe^{3+}$ support the high redox potential, $Co^{3+}$ can realize fast kinetics and $Mg^{2+}$ show a pinning effect to stabilize the structure with compatible radii. It presented a discharge capacity of 140 mAh $g^{-1}$ and superior capacity remain (about 95 mAh $g^{-1}$) after 500 cycles at 1 C in 2.5–4.0 V. Meanwhile, the high-rate performance also is excellent, which delivers a capacity of 118.2 and 73.9 mAh $g^{-1}$ at 5 C and 10 C, respectively. It can be explained by a wide capacity range (> 70%) of formed P3 and P'3 phases, in which prismatic paths can greatly enhance the $Na^+$ migration compared with octahedral paths resulting from O3 phases [86, 87]. The low $Na^+$ migration barrier (0.22 eV) resulting from DFT calculation also support this opinion. Some other elements substitution such as Ni [88, 89], Ti [90], Co [91, 92] have been reported, but the electrode performance is still unsatisfactory in long term lifespan or average operating voltage.

#### *1.1.2 O3-type $Na_xMnO_2$*

Mn-based cathode have received great attention due to the low cost and high abundance [93, 94]. $Na_xMnO_2$ with 2D structures have two polymorphs, which is classified into α-$NaMnO_2$ (space group C2/m) and β-$NaMnO_2$ (space group Pmnm) at low-temperature and high-temperature form, respectively [35, 95, 96]. α-$NaMnO_2$ is monoclinic O3 layered structure owing to Jahn–Teller distortion of $Mn^{3+}$ [51]. While β-$NaMnO_2$ has a zigzag layer structure, which is made up of two edge-sharing stacks of the $MnO_6$ octahedra and Na ion [97]. Thus, we will focus on the α-$NaMnO_2$ in the article. O'3-type α-$NaMnO_2$ as electrode materials, was first reported by Hagenmuller and co-workers [35] in 1985, there are reversible de/interealation at the Na content between 0.77 and 1.0 with large voltage hysteresis. It is due to high resistivity resulting from intrinsic semiconductor characteristic for α-$NaMnO_2$, which is also evidenced from first principles computations [98].

In 2011, Ceder et al. [51] revisited the monoclinic α-$NaMnO_2$, it delivers 185 mAh $g^{-1}$ of reversible capacity at 0.1 C rate in the voltage range of 2.0–3.8 V, corresponding to 0.8 mol Na intercalated back. The charge–discharge curves have a character of muti-plateaus indicating different reaction paths with different intermediate phase. However, it only remains a capacity of 132 mAh $g^{-1}$ after 20 cycles, mainly resulting from strong Jahn–Teller effect of $Mn^{3+}$. According to crystal field theory, the Jahn–Teller effect is related to the distribution of transition metal d electrons in the energy level. In octahedral structure, the d orbits are divided into low-energy orbits $t_{2g}$ ($d_{xy}$, $d_{zx}$ and $d_{yz}$) and high-energy orbits $e_g$ ($d_z^2$ and $d_x^2$-$_y^2$). The electrons occupy the d orbits in the order of low to high energy. Three outermost layer electrons of $Mn^{3+}$ occupy preferentially the orbit $t_{2g}$ and another electron occupies the $d_z^2$ or $d_x^2$-$_y^2$ orbits, which generally produce elongated or compressed distortions, leading to distortion of the layered structure. Such distortions are usually detrimental to structural stability and may be accompanied by $Na^+$/vacancy ordering [22, 99, 100]. Thus, it is essential to regulate Jahn–Teller effect to improve the cyclic stability. Li et al. [52] designed a O'3-$NaMn_{0.6}Al_{0.4}O_2$ cathode with queue-ordered superstructure (Fig. 3d). On the one hand, the special superstructure reinforces the layer structure and decrease the harmful effect from Jahn–Teller distortion. On the other hand, the $Mn^{3+}$ migration from transition metal layer to Na layer is restrained. Thus, it delivers a modest capacity of 160 mAh $g^{-1}$ and enhanced rate and cyclic performance, compared with the O'3-$NaMnO_2$. In addition, the queue-ordered superstructure is demonstrated that it has the lowest energy and strengthen ionic bonds between Mn and O by DFT calculations, which can increase the

structure stability during cycles, which further supports the improved cyclic performance. The anionic redox chemistry has been developed in Li-rich materials due to the additional capacity delivery along with higher energy. However, it usually accompanied with $O_2$ release in the high voltage regions owing to the weak covalence bond from 3d transition metal. Zhou's group [53] predicted that Ir doping in Mn-based cathode has the most favorable oxygen absorption and compared with Cd and Ru doping by DFT calculations, and increasement of Mn 3d band as well as large hybridization between Ir and O can effectively decrease $O_2$ release (Fig. 3e). Based with the deduction, they prepared $Na_{1.2}Mn_{0.4}Ir_{0.4}O_2$ O3-type Na-rich materials, which delivers a capacity of 179 mAh $g^{-1}$ in the voltage range of 1.5–4.4 V by employing cationic and anionic redox. The highly reversible O redox was confirmed by in operando Raman and XAS tests. It provides a new strategy to increase the capacity delivery for Mn-based cathode. Cho and co-workers [101] employ first-principles calculations to predict electrochemical performance for $Na(Li_{1/3}Mn_{2/3})O_2$ cathode. It shows high redox potentials (≈4.2 V vs Na/Na+) with high charge capacity (190 mAh $g^{-1}$) resulting from the anionic redox reactions.

Moreover, multielement co-doping can also effectively improve the cyclic performance, average operating voltage, energy density and so on depending on synergistic effect. Deng [54] synthesized an air-stable $Na[Li_{0.05}Mn_{0.50}Ni_{0.30}Cu_{0.10}Mg_{0.05}]O_2$ cathode by coprecipitation method and proposed that Li and Mg are contributing to enhancement of electronic conductivity, Cu can improve the surface structure and regulate phase transition, leading an outstanding air stability, Inactive Mn and Li substitution can remain structure stability. It delivers a discharge capacity of 172 mAh $g^{-1}$ and superior rate capacity up to 50 C. After 1000 cycles at 20 C, 70.4% capacity retention was maintained, which surpass many other reported O3-type cathode. The pouch cell assembled by this cathode/hard carbon delivers discharge capacity of 70 mAh $g^{-1}$ and good stability. Recently, a O3-type $Na_{0.5}Mn_{0.65}Ni_{0.15}Al_{0.1}Mg_{0.05}Co_{0.05}O_2$ nanoflower [102] was presented based on multi-metal synergetic mechanism, in which $Al^{3+}$ and $Mg^{2+}$ have a positive effect on structure stability, $Co^{2+}$ can enhance rate capacity, $Ni^{2+}$ and $Mn^{3+}$ is mainly responsible for charge compensations. A capacity loss of only 0.018% in every cycle was realized after 1000 cycles at 1 C.

#### *1.1.3 O3-type $Na_xNiO_2$*

$NaNiO_2$ is stable in two polymorphs: a low-temperature layered O3 structure with a monoclinic distortion, and a high-temperature rhombohedral phase. Monoclinic $NaNiO_2$ (space group: C2/m) has been studied extensively owing to the relatively high voltage platform and redox reaction [103]. The structure is categorized as O'3 due to the Jahn–Teller effect of low spin of $Ni^{3+}$ (t6 2 g e1 g), which is composed of alternately stacked Ni–O layer containing edge sharing elongated $NiO_6$ octahedra and Na layer [104, 105]. Ceder [55] investigated electrochemical deintercalation of sodium from $NaNiO_2$ in 2012. It delivers a capacity of about 120 mAh $g^{-1}$ in 1.25–3.75 V with multiple plateaus, corresponding to 0.52 mol Na back. The complex phase transitions O'3-P'3-P"3-O"3-O"'3 is confirmed by in situ XRD [103, 106]. When cycle in 2.0–4.5 V, it shows significant capacity decline in several deintercalation/intercalation, which is due to the formation of an inactive phase at high voltage zone. Unfortunately, the phase can't be identified. Recently, to understand in depth the structural evolution along with irreversible capacity loss in high voltage, Wang et al. [107] visually observed the structural evolution process by in operando TXM-XANES. It exhibits a dissymmetric spatial distribution with a "core–shell" reaction mechanism and one irreversible phase ($Na_{0.17}NiO_2$) result in discrepant intercalation (Fig. 4a, b). The irreversible capacity loss is resulting from two regions, below 3.0 V and above 4.0 V. The former is caused by increased c spacing after the first charge process whereas it cannot shrink back. The latter are affirmed to owing to unrecoverable lattice distortion and possible electrolyte decomposition. Therefore, it is vital to adopt effective strategy such as cation-doping or optimizing cutoff voltage to obtain higher reversibility and structure stability.

It is worth pointing out that pristine $NaNiO_2$ still shows inferior cycle stability and reversibility, and it is very hygroscopic against moist atmosphere, which slow down their practical application in sodium ion batteries. Many investigations have confirmed transition metal substitution have the positive effect in electrochemistry performance, such as $Na_{0.8}Ni_{0.6}Sb_{0.4}O_2$ [56, 108], $NaNi_{1-y}Co_yO_2$ [109–111], $Na_{0.7}Ni_{0.35}Sn_{0.65}O_2$ [57, 112], $NaNi_{0.5}Ti_{0.5}O_2$ [58, 113]. Xu et at. prepared a $Na_{0.8}Ni_{0.6}Sb_{0.4}O_2$ cathode [56], delivering a capacity of 106 mAh $g^{-1}$ at 0.1 C based on the $Ni^{2+}/Ni^{3+}$ redox couple along with a high average working voltage of 3.5 V, which is due to the reduced orbital hybridization between O 2p and M 3d. In addition, the phase evolution process was believed to simplified O3-P3 with small volume change (1.0%), thus shows an excellent cycling life, compared with $NaNiO_2$ [106]. However, the rate performance is inferior may resulting from poor electronic conductivity. Trivalent cobalt also can suppress the cooperative Jahn–Teller distortion and enhance structure stability, whereas the content of cobalt haves to exceed 0.22 ($NaNi_{1-y}Co_yO_2$). It is well-established that the price of cobalt is expensive and the distribution is uneven in the earth's crust. Overmuch cobalt

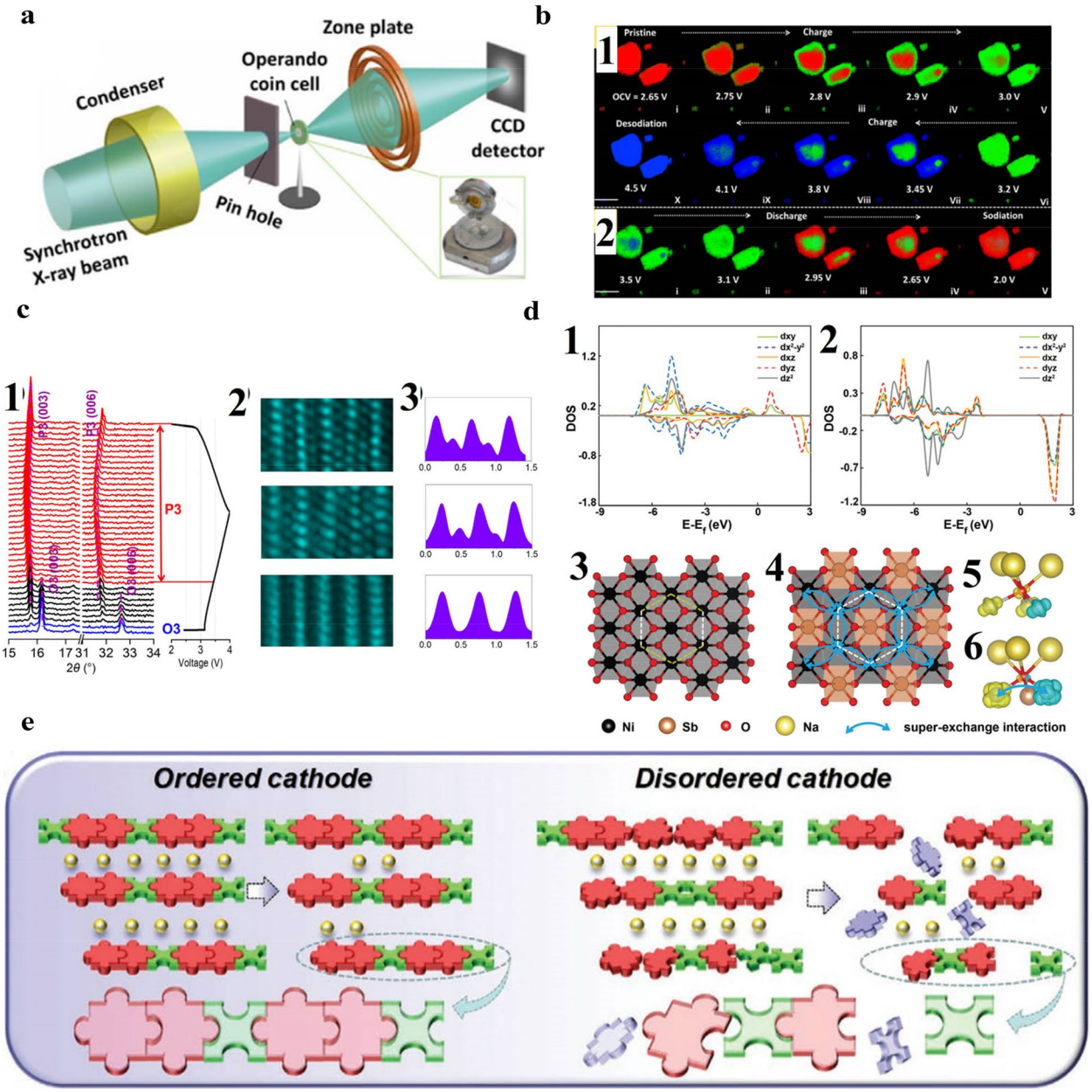


**Fig. 4** **a** Schematic illustration of the TXM experimental setup. **b** $b_1$ and $b_2$ are the two-dimensional chemical phase mapping during the first charge and discharge process. Scale bar: 10 μm. Reproduced with permission [107]. Copyright 2017, Elsevier B.V. **c** $c_1$ In-situ XRD patterns collected for NNCT electrode cycled in the voltage range of 2.0–4.0 V. The O3-type phase, biphase coexistence, and P3-type phase are represented by blue, black, and red colors, respectively. $c_2$ STEM images of the pristine (bottom), fully charged (middle), and fully discharged (top) NNCT electrodes viewed along the [0 1 0] direction. $c_3$ The corresponding line profiles of the STEM images. Reproduced with permission [59]. Copyright 2018, Elsevier B.V. **d** $d_1$ and $d_2$ The partial density of states (pDOS) of $NaNiO_2$ and $NaNi_{2/3}Sb_{1/3}O_2$. $d_3$ and $d_4$ The comparison of bond length of $NaNiO_2$ and $NaNi_{2/3}Sb_{1/3}O_2$ structure. $d_5$ and $d_6$ The spin difference charge density of $NaNiO_2$ and $NaNi_{2/3}Sb_{1/3}O_2$. Reproduced with permission [117]. Copyright 2019, Wiley–VCH. **e** Schematic diagram showing that the ordered arrangement of transition metal (TM) in layered oxide could provide a more stable structure for long-term (de)intercalations of Na + in comparison with that of the disordered arrangement. Reproduced with permission [61]. Copyright 2020, Wiley–VCH

addition will make Na-ion batteries lose competitiveness compared with Li counterpart.

Guo et al. [57] introduce Sn into Ni-based layered oxide, it shows the highest redox potential of 3.7 V among all O3-type cathode. It can be explained by electronic structure and molecular orbitals. $Sn^{4+}$ ([Kr] $4d^{10}$) does not hybridize with O 2p orbitals due to no single d electrons. Orbital hybridization only exists in O 2p orbitals and Ni $e_g$ orbitals and charge delocalization is thus prevented in the metallic layer, leading to an increasement of Ni–O bond ionicity and Ni redox reaction. In contrast, other traditional transition metals (M') substitution such as Fe, Mn, O 2p orbital hybridization can simultaneously happen with both Ni $e_g$ and M' $e_g$, thus the contribution from the Ni $e_g$ orbital became smaller, resulting in a relatively lower voltage. The charging and discharging curve is smooth and shows a considerably flat platform. Unfortunately, the reversible capacity is only 64 mAh $g^{-1}$ in 2.0–4.0 V, which is relevant to internal Na-deficient (0.7).

It is confirmed that titanium as structure stabilizer can reduce the series of structural changes and increase the average potential, compared to half cells using $NaNiO_2$ cathodes. The discharge curves of $NaNi_{0.5}Ti_{0.5}O_2$ is composed of a slope and a platform rather than multistep potential curve [113]. Zhou's research [58] demonstrated its good performance delivery with a reversible specific capacity of 102 mAh $g^{-1}$ at 0.2 C and capacity retention of 75% at 1 C after 300 cycles in the voltage range of 2.0–4.0 V, which is well ahead of $NaNiO_2$. The full-cell assembled by $NaNi_{0.5}Ti_{0.5}O_2$/ pre-sodiated hard carbon delivers a reversible capacity of 93 mAh $g^{-1}$ and good cyclic performance. However, the phase of $NaNi_{0.5}Ti_{0.5}O_2$ is always accompanied by a small quantity of NiO about 7 mol %, which is inevitable regardless of all synthesis conditions. Recently, Zhou's group [59] design a cation-mixing stabilized cathode ($Na_{0.8}Ni_{0.3}Co_{0.1}Ti_{0.6}O_2$) by composition adjustment. It is verified that there is a typical phase transformation of O3-P3 in the first charge along with cation mixing. However, it unexpectedly maintains the P3 structure in the subsequent cycles (Fig. 4c), which is due to the TM ions in Na layers have a grasp effect on TM sheets. P3-type structure with trigonal prismatic sites can enable fast $Na^+$ migration compared to the octahedral sites in O-type structure, thus can deliver great rate capability. In addition, the P3-type structure shows an extremely low lattice strain in desodiation and sodiation. Therefore, it delivers an excellent rate capability and superior capacity retention of 98% at 5 C after 1000 cycles. More recently, they presented reversibility of phase transition is highly relevant to oxygen vacancy concentrations and thus have a crucial role on electrochemistry performance [60]. The synthetic $Na_{0.9}Ni_{0.3}Co_{0.15}Mn_{0.05}Ti_{0.5}O_2$ sample in $O_2$ atmosphere have abundant oxygen vacancies but the oxygen vacancy decreases in Ar atmosphere. The vacancy-rich sample process an irreversible phase transition of O3-P3. However, the vacancy-poor sample is a mixed phase containing O3 and partial P3 after cycling. In other words, it is irreversible process. Moreover, the electronic and ionic conduction are facilitated due to incorporation of oxygen vacancy. As expected, it shows the splendid rate capability (about 50 mAh $g^{-1}$ at 100 C) and excellent cycling performance (capacity retention of 81.6% over 1000 cycles).

Recently, the new material families of $Na_3Ni_2XO_6$ (X = Sb, Bi, Ru, etc.) are presented owing to the superior structure stability and long lifespan [61, 62]. Unlike disordered Ni-based layer oxides, the $Ni^{2+}$ and $X^{5+}$ are preferably formed an ordered distribution within the transition metal layers due to the unique proportion (2:1) and notably different ionic radius, thus usually form honeycomb layered structure with ordered superlattice [114, 115], where each $XO_6$ octahedron is surrounded by six edge-sharing $NiO_6$ octahedra in the "ab" plane. It is worth pointing out that there are some weak reflections around $2\theta = 20°$ in the XRD pattern based on the C2/m model, which is different from the diffraction peaks resulting from O3-type structure [116]. Honeycomb-layered $Na_3Ni_2SbO_6$ was first applied for an cathode in 2014 [62], it shows a capacity of about 120 mAh $g^{-1}$ based on $Ni^{2+/3+}$ redox couple along with an average high working voltage at 3.3 V. Meanwhile, the rate and cyclic performance are superior compared to the $NaNiO_2$. However, the underlying mechanism is still not clear. Recently, Guo's group [117] revisited the $NaNi_{2/3}Sb_{1/3}O_2$ and presented that ordered $Ni_6$-rings with super-exchange interaction form symmetric atomic configuration and degenerate electronic orbital in layered oxides (Fig. 4d), thus enhancing the structural stability in terms of air, thermal and phase stability, which is also supported by DFT calculations. In addition, the redox potential was increased and phase-transition process became simply compared with pristine $NaNiO_2$. Zhou's group developed the superlattice-stabilized layered oxide cathode ($Na_3Ni_2RuO_6$) [61], which shows an ultralong voltage platform and a high discharge capacity of 130 mAh $g^{-1}$ along with reversible O3 to P3 phase transition. Meanwhile, it also presents excellent capacity retention (81%) after 1000 cycles with cation-migration-free. So stable structure can be explained visually by a "puzzle model". TM ions can generate an interactive force resulting from ordered honeycomb-type arrangement, thus modify the crystal strain and remain the structural integrity during the numerous desodiation and sodiation (Fig. 4e). However, due to the price of raw material ($RuO_2$) is very

expensive and abundance is low (only 0.001 ppm in the earth's crust), so it may be not suitable for large-scale commercial application.

#### *1.1.4 O3-type $Na_xNi_yMn_{1-y}O_2$*

$NaNi_{0.5}Mn_{0.5}O_2$ is a typical O3-type layered cathode, which was first developed by Komaba [32] in 2009. It shows great potential to achieve commercial application relying on high discharge capacity resulting from $Ni^{2+/3+/4+}$ redox couple, low cost for inactive $Mn^{4+}$ and facile synthesis. It is worth pointing out that there is not almost cation mixing in $NaNi_{0.5}Mn_{0.5}O_2$ due to the comparatively different ion sizes of $Na^+$(1.02 Å) and $Ni^{2+}$(0.69 Å), compared to the Li counterpart $LiNi_{0.5}Mn_{0.5}O_2$ which containing $Li^+/Ni^{2+}$ disordering, thus making sure the better ion transfer [118]. In the voltage ranges of 2.2–3.8 V, it delivers a high reversible capacity of 125 mAh $g^{-1}$ at the current density of 4.8 mA $g^{-1}$. When the upper voltage is 4.5 V, a capacity delivery of 185 mAh $g^{-1}$ is realized, but the capacity deteriorated only after 20 cycles. The charging and discharging curve contained several potential plateaus resulting from sliding of slabs and $Na^+$/vacancy ordering [119]. A structure evolution of O3-O'3-P3-P'3-P"3 was determined by ex situ X-ray diffraction [31]. Komaba presented fluorinated ethylene carbonate [120] as an electrolyte additive can effectively improve coulomb efficiency and cycling stability owing to the passivation and suppression of side reactions. The full cell $NaNi_{0.5}Mn_{0.5}O_2$ /hard carbon delivered a high capacity over 200 mAh $g^{-1}$ (based on negative electrodes) along with operating voltage of about 3 V. Even though the current density is 300 mA $g^{-1}$, it remains an almost similar capacity. Another full cell employed with Sn–C as anode [121] presented a high energy density of 300 Wh $kg^{-1}$ with good retention, further confirms commercial potential of $NaNi_{0.5}Mn_{0.5}O_2$.

Although $NaNi_{0.5}Mn_{0.5}O_2$ cathode materials show excellent superiority, some shortages have to be overcame for commercialization progress. Multiple phase transformation not only induce stepwise plateaus leading an unstable power export, but also disturb diffusion of sodium owing to the TM ions in different sites, leading terrible rate and cyclic performance [21, 94]. Thus, suppressing phase transition and extending solid solution zone by appropriate elements addition can effectively alleviate the above problems. In addition, the intrinsic hygroscopic is also a crucial factor to hinder their commercial application, which will increase production and storage costs along with performance degradation. The Na-deficient phase is formed due to the spontaneous $Na^+/H^+$ exchange in ambient air [122, 123]. Meanwhile, some insulating alkaline species such $Na_2CO_3$ and $NaHCO_3$ on the surface of bulk particle can decrease capacity delivery and trigger gelation of the slurry [124–126]. Proper elements substitution and surface modification can improve the problem.

Wang et al. [63] apply partial Ti to replace Mn in $NaNi_{0.5}Mn_{0.5}O_2$. Due to the similar ionic radius and same valence, it still maintained O3-type structure along with homogeneous distribution after introduction of Ti. Series of sodium-sufficient O3-$NaNi_{0.5}Mn_{0.5-x}Ti_xO_2$ ($0 \le x \le 0.5$) materials was investigated and it can be concluded that $NaNi_{0.5}Mn_{0.2}Ti_{0.3}O_2$ cathode delivers the best electrochemical performance, which presents a high discharge capacity of 134 mA h $g^{-1}$ at 0.05 C in 2.0–4.0 V along with 85% capacity retention at 1 C after 200 cycles based on $Ni^{2+}/Ni^{3+}$ active redox couple. Meanwhile, the charge/discharge profiles become smoother and plateau potential is increased. The desodiation and sodiation process is corresponding to O3 − P3 transition via gliding of the $TMO_2$ layers (Fig. 5a). In other words, the Ti incorporation in O3-type $NaNi_{0.5}Mn_{0.5}O_2$ suppress the multiple phase transformation and decrease of the energy barrier for the two-phase conversion, leading a highly reversible phase transition along with excellent rate and cyclic performance. Komaba et al. [127] presented Mg and Ti co-substituted cathode $Na[Ni_{4/9}Mn_{1/3}Mg_{1/18}Ti_{1/6}]O_2$, which delivers a better capacity of 200 mAh $g^{-1}$ without any capacity loss due to substitution and enhanced cyclic performance in the voltage range of 2.2–4.5 V. In contrast to the $NaNi_{0.5}Mn_{0.5}O_2$, it demonstrates delayed O3-O'3 transition and decreased lattice parameter mismatch between O3 and P3 phases, resulting in gradual structural changes along with smoother curves. Furthermore, an OP2-like P–$O_e$–$O_f$ intergrowth phase as an intermediate buffer phase effectively suppress the dramatic shrinkage in interslab spacing, leading a high reversibility of structure (Fig. 5b). After cycling, the surface of Mg and Ti co-substituted cathode is as smooth as pristine, but the surface deterioration is significant for $NaNi_{0.5}Mn_{0.5}O_2$. Hong and co-workers [128] demonstrated that Al-doped effectively facilitate $Na^+$ mobility and improve structural stability due to increasement of the interslab distance resulting from stronger Al − O bond. O3-$NaAl_{0.02}Ni_{0.49}Mn_{0.49}O_2$ presented a high capacity retention of 63.2% after 200 cycles at 1 C along with coulombic efficiency of over 99% in the voltage range of 2.0–4.0 V. Recently, $Zn^{2+}$ doping [64] is verified that can not only enhance electrochemical reversibility in the high voltage range of 4–4.2 V, but also improve air stability. The O3-$NaNi_{0.47}Zn_{0.03}Mn_{0.5}O_2$ cathode presents a reversible capacity of 113 mAh $g^{-1}$ at 0.5 C and good capacity retention. It is worth mentioning that a small volume change of approximately 2.00% in the voltage range of 2–4 V

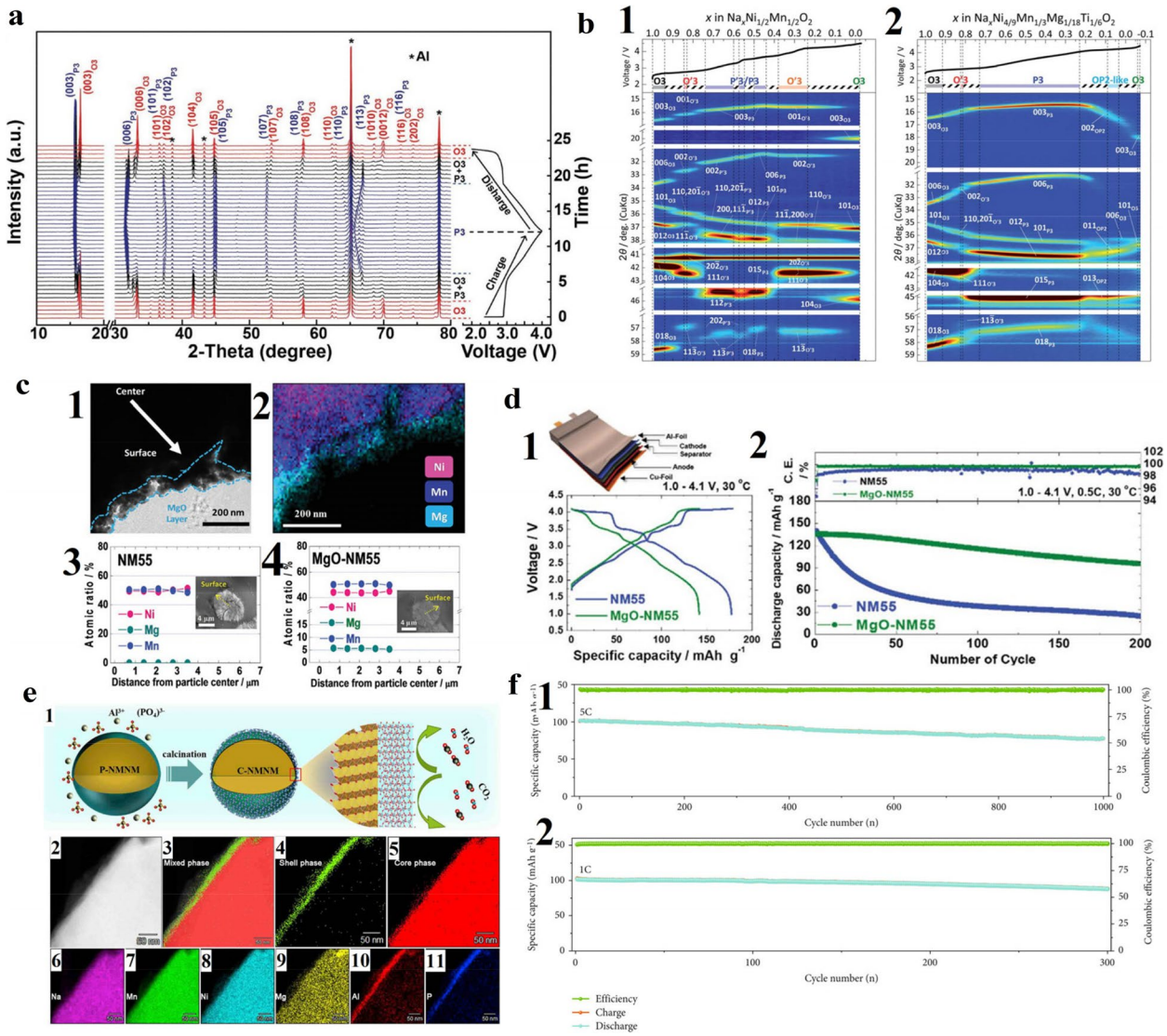


**Fig. 5** **a** In situ XRD patterns collected during the first charge/discharge of the Na/$NaNi_{0.5}Mn_{0.2}Ti_{0.3}O_2$ cell under a current rate of 0.05 C at voltage range between 2 and 4 V. Black asterisks represent peaks from Al window. Reproduced with permission [63]. Copyright 2017, Wiley–VCH. **b** Contour plots of operando XRD patterns for $b_1$ Non-sub and $b_2$ Mg–Ti-sub electrodes during 1st charging to 4.5 V. Reproduced with permission [127]. Copyright 2021, Royal Society of Chemistry. **c** $c_1$ Bright field TEM image and $c_2$ corresponding EDS mapping of MgO-NM55. EPMA results of $c_3$ NM55 and $c_4$ MgO-NM55 cathodes. Inset images display the cross-sectional SEM images of NM55 and MgO-NM55 particles, respectively. **d** Electrochemical performances of pouch-type NM55/hard carbon and MgO-NM55/hard carbon full cells: $d_1$ initial charge–discharge voltage profiles at 15 mA $g^{-1}$ and $d_2$ coulombic efficiency and long-term cycling stability test at 0.5 C-rate (75 mA $g^{-1}$). Reproduced with permission [66]. Copyright 2018, Royal Society of Chemistry. **e** $e_1$ Schematic illustration of the synthetic process for the $AlPO_4$ coating on the surface of $Na[Li_{0.05}Mn_{0.50}Ni_{0.30}Cu_{0.10}Mg_{0.05}]O_2$. $e_2$ High-angle annular dark field (HAADF)-STEM image. STEM-EDS mapping of crystalline phase: Mixed phase of C-NMNM $e_3$, $AlPO_4$ shell phase $e_4$ and core phase of $Na[Li_{0.05}Mn_{0.50}Ni_{0.30}Cu_{0.10}Mg_{0.05}]O_2$ ($e_5$). ($e_6$-$e_{11}$) Element Na ($e_6$), Mn ($e_7$), Ni ($e_8$), Mg ($e_9$), Al ($e_{10}$) and P ($e_{11}$) distributions from the edge to the bulk material of C-NMNM. Reproduced with permission [129]. Copyright 2019, Cell Press. **f** $f_1$ Cycling performance during 1000 cycles at 5C after performance tests at various rates. $f_2$ Electrochemical performance of full-cell system Cycling performance during 300 cycles at 1C. Reproduced with permission [134]. Copyright 2020, American Association for the Advancement of Science

was demonstrated. Meanwhile, the average sodium ion diffusion coefficients of $Zn^{2+}$ doping cathode is $2.22\times10^{-10}$ $cm^2$ $s^{-1}$, which far beyond the pristine sample ($1.37\times10^{-12}$ $cm^2$ $s^{-1}$). Tarascon [65] replaced $Mn^{4+}$ by a non-transition metal ion $Sn^{4+}$, preparing a series of $NaNi_{0.5}Mn_{0.5-y}Sn_yO_2$ (y = 0–0.5). It is believed that $Sn^{4+}$ substitution could reduce orbital overlap, favor charge localization in the metallic layer and increase bond ionicity, resulting in higher redox potential. Moreover, destabilization of P3 phase could suppress

the phase transition from O3 to P3 due to increasing the ionic nature of the crystal lattice. Thus, it is a promising strategy to simultaneously increase the redox voltage and delay the phase transition. The fully substituted $NaNi_{0.5}Sn_{0.5}O_2$ phase shows a high redox potential of ≈3.2 V with a single-phase transition from O3 − P3. When y = 0.4, $NaNi_{0.5}Mn_{0.1}Sn_{0.4}O_2$ cathode delivers a capacity of 91 mAh $g^{-1}$ and superior capacity retention (85% after 200 cycles). However, $H_2O$ insertion is present after $Sn^{4+}$ substitution due to the increased interlayer distance, the application has been limited a certain extent.

Surface coating is considered an effective way to suppress the unfavorable side reactions during cycling and remain structure stability. Hwang [66] prepared MgO coating $NaNi_{0.5}Mn_{0.5}O_2$ with partial Mg doping. The coating layer of 70–100 nm formation on the particle surface effectively prevent the bulk particle HF erosion. Meanwhile, $Mg^{2+}$ incorporation into the transition metal (TM) layers reduce the extent of the irreversible multiphase transformation (Fig. 5c). In the voltage range of 2.0–4.2 V, the MgO coating $NaNi_{0.5}Mn_{0.5}O_2$ shows improved capacity retention of 75% after 100 cycles at 0.5 C, though the discharge capacity slightly decreases due to the inactive MgO. The pouch-type full cells were assembled with MgO coating $NaNi_{0.5}Mn_{0.5}O_2$ and hard carbon, delivers excellent capacity retention of 70% after 200 cycles at 1.0–4.1 V (Fig. 5d). Zhang [129] performed a surface modification process by a rotary evaporator, which make $AlPO_4$ protective layer uniformly deposit on the cathode material (Fig. 5e). It can protect bulk particle from corrosion of electrolyte, decrease transition metal dissolution, and remain crystal structure. Meanwhile, it can protect the anode from increased resistance by suppressing the dissolution-migration-deposition process. The half-cell and full-cells show excellent cycling lifespan (95% after 400 cycles at 1 C, 78% after 200 cycles at 1 C, respectively) (Fig. 5f). In addition, the protective layer can further improve its environmental stability. Atomic layer deposition (ALD) technology is an effective way to realize surface coating at atomic scale with a precise and uniform thickness control, have been widely applied in many energy storage systems [7, 130–132]. Yang [133] prepared thin $Al_2O_3$ coating (about 3 nm) $NaNi_{0.5}Mn_{0.5}O_2$ via ALD, which presents an excellent capacity retention of 68.0% after 300 cycles at 0.5 C, along with improved rate capability. In addition, the air sensitivity test was performed and showed more stable structure compared to the pristine sample. There is obvious impurity and hydrated compounds formation in the uncoated sample by XRD analysis. So, the $Al_2O_3$ layer effectively avoid the direct contact of ambient atmosphere, leading less degradation (Fig. 6a). Although the cyclic performance of layer cathode is obviously improved, it's essential to point out that most of coating layers are electrochemically insulated and discharge capacity is decreased, leading a lower energy density to a certain extent.

Hygroscopic characteristic is a crucial factor to hinder their commercial application. The spontaneous $Na^+/H^+$ exchange is easily happened in the O3-type $NaNi_{0.5}Mn_{0.5}O_2$ cathode in ambient air [122, 123]. As the interlayer spacing become larger due to the increased repulsion between adjacent oxide layers, more $Na^+$ are extracted, eventually resulting in a Na-deficient phase and deteriorative electrode performance[21]. Meanwhile, some insulating alkaline species on the surface of bulk particle are formed [124, 125]. On the one hand, they decrease capacity delivery and deteriorate rate and cyclic performance. On the other hand, they will trigger defluorination of polyvinylidene fluoride (PVDF) binder, then cause the gelation of the slurry and rough surface, impeding their practical viability [135]. Surface coating strategy can avoid cathode exposing in ambient air containing $H_2O$ and $CO_2$ to a certain extent. But it is usually accompanied by decreased energy density. Yao [11] designed an air-stable O3-type cathode $NaNi_{0.45}Cu_{0.05}Mn_{0.4}Ti_{0.1}O_2$ by Cu/Ti co-substitution, in which Cu has comparable electronegativity and Ti has substantial difference in Fermi level compared to the $Ni^{2+}/Mn^{4+}$, resulting in contractions of Na layers and increasement of the valence state of Ni. After exposed to air for 2 days, the structure is not almost changed and even retains its structure after being soaked in water (Fig. 6b). In contrast, O'3 and P3-type $Na_{1-y}Ni_{0.5}Mn_{0.5}O_2$ phase arose just after 2 h for $NaNi_{0.5}Mn_{0.5}O_2$ cathode resulting from spontaneous $Na^+$ extraction and insertion of $H_2O$ molecules. In addition, $NaNi_{0.45}Cu_{0.05}Mn_{0.4}Ti_{0.1}O_2$ still shows high capacity retention after aging experiments. The Cu/Ti co-substitution cathode shows higher reversible capacity along with smoother discharge/charge curves and significantly enhanced cyclic performance (70.2% of capacity retention after 500 cycles). The phase transition was determined by in situ XRD, corresponding to highly reversible O3-P3 evolution, thus Cu/Ti co-substitution also effectively suppressed complex multistage evolution. Xiao [134] incorporate $Mg^{2+}$ into the $NaNi_{0.45}Cu_{0.05}Mn_{0.4}Ti_{0.1}O_2$ cathode. The $NaNi_{0.40}Cu_{0.05}Mg_{0.05}Mn_{0.4}Ti_{0.1}O_2$ cathode presents outstanding capacity retention of 76.4% after 1000 cycles at 5 C and a stable midpoint voltage (Fig. 6c). Meanwhile, the O3-type phase could be maintained after 3 days (Fig. 6d). Zheng [136] demonstrated that ethanol washing can remove most of the alkaline species such as $Na_2CO_3$ and $NaHCO_3$ and remain original $NaNi_{0.5}Mn_{0.5}O_2$ structure.

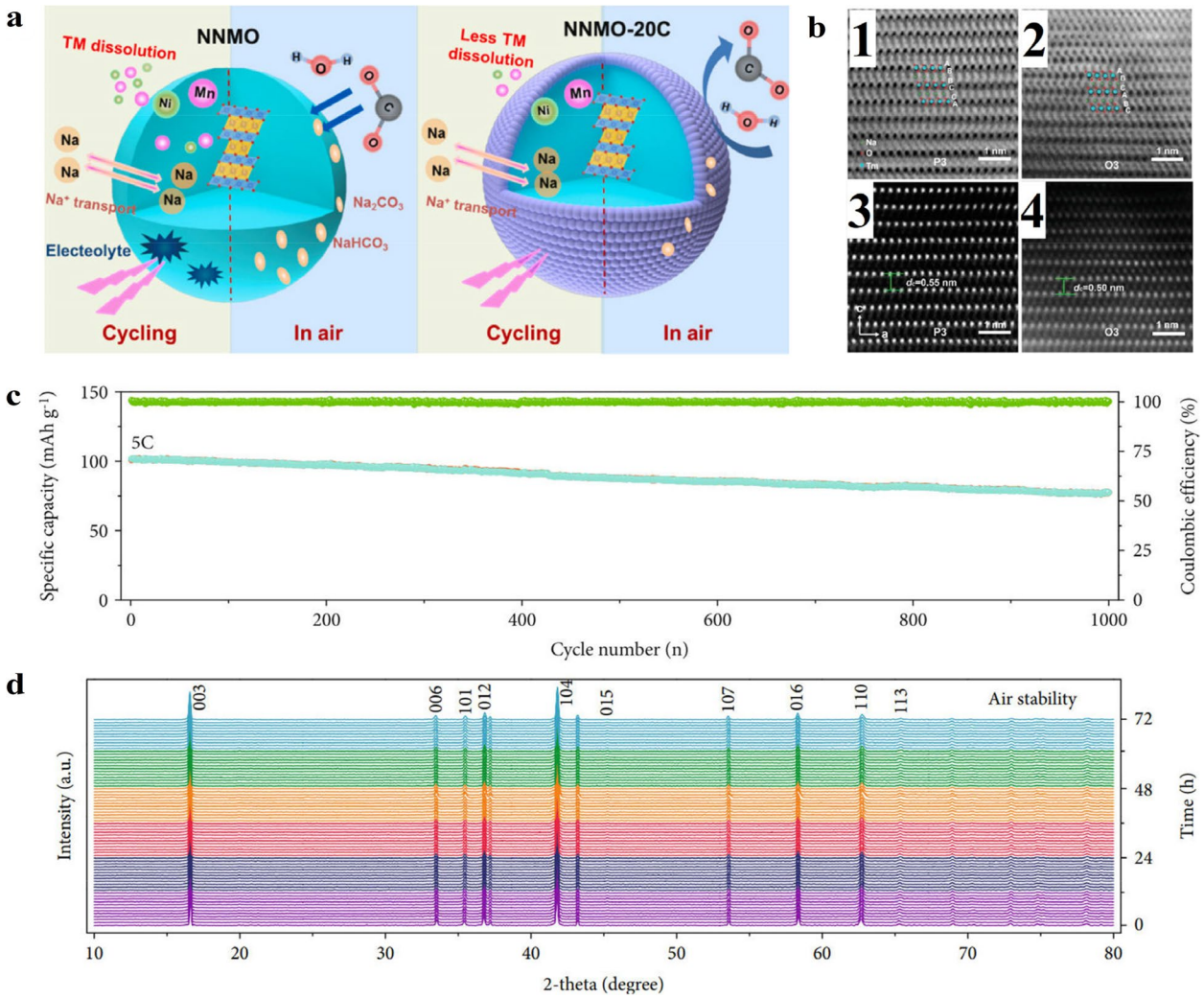


**Fig. 6** **a** Schematic illustration of the advantages for the $Al_2O_3$-surface modification in stabilizing the surface and bulk structure of the NNMO cathode. Reproduced with permission [133]. Copyright 2019, Elsevier B.V. **b** ABF-STEM images of water-soaked ($b_1$) NaNM and ($b_2$) NaNCMT. HAADF-STEM images ofwater-soaked ($b_3$) NaNM and ($b_4$) NaNCMT. Reproduced with permission [11]. Copyright 2018, American Chemical Society. **c** Cycling performance during 1000 cycles at 5C after performance tests at various rates. **d** In situ XRD patterns of air-exposure stability test for three days (the different colour regions stand for the different air-exposure stages). Reproduced with permission [134]. Copyright 2020, AAAS

### *1.1.5 O3-type $Na_xNi_yMn_zFe_{1-y-z}O_2$*

Although O3-type Ni-Mn based oxides are superior to other oxides, but their practical application is limited by irreversible multiple phase transformation and hygroscopic characteristic. The frequent irreversible phase transitions are mainly due to the lack of shielding by the electrostatic repulsion of lattice oxygen and the gliding of transition metal layers. The hygroscopic characteristic is mainly related to the excess surface residual alkali and the large layer spacing, resulting in the insertion of water into the layered structure. In addition, the price of nickel is also rising year by year, which may trigger higher raw material costs, and it is necessary to properly reduce the Ni content and use low-cost element substitution. Among many elements, Fe has the advantage of low cost and the ionic radius is similar to Ni and Mn, which may be easily introduced into the NiMn-based material to reduce layers gliding. Yuan [67] prepared a serious of Fe-substituted $NaNi_{0.5}Mn_{0.5}O_2$ cathode materials. It is confirmed that Fe substitution to Ni-Mn layered oxide not only could effectively suppress the suppression of $MO_2$ gliding and Na/vacancy ordering resulting in reversible O3-P3 transformation, but also could expand the interslab distance which leads to fast ionic diffusion. The O3-type $NaFe_{0.2}Mn_{0.4}Ni_{0.4}O_2$ showed smoother the charge/discharge profiles compared with $NaNi_{0.5}Mn_{0.5}O_2$

and remarkably improved cycle stability with a capacity retention of 96.4% after 30 cycles in a voltage range of 2.0–4.0 V. A superior reversible capacity of 133, 133, 131, 125, 120, 112, 100, and 86 mAh $g^{-1}$ at current rates of 0.05, 0.1, 0.2, 0.5, 1, 2, 5 and 10 C (1 C = 240 mA $g^{-1}$) were also delivered. Furthermore, in the high voltage range (> 4.0 V), the O3-type $NaFe_{0.2}Mn_{0.4}Ni_{0.4}O_2$ undergo a different OP2 phase transformation with smaller interslab distance (5.13 Å) than the P3" phase in $NaNi_{0.5}Mn_{0.5}O_2$ (5.72 Å), which effectively restrain co-insertion of the electrolyte solvent, leading improved cyclic performance. Sun et al. [137] proposed that with Fe contents increasement in the Ni–Fe-Mn based materials, the electrode exhibits more stable cyclic performance and perfect thermal stability although the reversible capacity slightly decreases. This further proves that addition of Fe has a positive effect on stabilization on crystal structure. Based on the DFT calculations, Guo et al. [68] proposed $Fe^{3+}$ with slightly larger radius is introduced into $NaNi_{0.5}Mn_{0.5}O_2$ could enlarge transition metal layers and facilitate electronic delocalization. The phase transformation process of the $NaFe_{0.3}Ni_{0.35}Mn_{0.35}O_2$ is single O3 − P3 without any monoclinic distortion (Fig. 7a). The capacity retention ratio of $NaFe_{0.3}Ni_{0.35}Mn_{0.35}O_2$ could reach 80% after 100 cycles at 1 C (1C = 240 mA $g^{-1}$) within 2.0 − 4.0 V voltage range and the rate performance were also obviously enhanced. In addition, the air stability of Ni–Fe-Mn based materials was effectively improved and it remained the O3 crystal structure after exposed to air for 1 day which was verified by directly at atomic-scale by ABF-STEM. Due to the excellent performance and lower price of Ni–Fe-Mn based material, the commercialization process is also advancing, Ma's group [27] realized kilogram-scale production of $NaFe_{1/3}Ni_{1/3}Mn_{1/3}O_2$ material by co-precipitation method and following calcination, which widely used in the production of layered oxide cathode materials for lithium-ion batteries. Meanwhile, they successfully prepared 1 Ah soft-packed batteries using $NaFe_{1/3}Ni_{1/3}Mn_{1/3}O_2$ and hard carbon as cathode and anode, respectively. It remains outstanding long term cycling performance with capacity retention over 73% after 500 cycles between 1.5 V and 3.8 V at 1C rate (Fig. 7b). The corresponding XRD diffraction pattern is almost same as the initial sample, further demonstrating its excellent structural stability. Afterwards, they used optimized electrolyte [28] (1 M $NaPF_6$ in 1:1 PC-EMC with 2wt% FEC, 1wt% PST, and 1wt% DTD) to enhance the long cycling life with 92.2% capacity retention after 1000 cycles at 1C. On the one hand, the PST and DTD additives can produce more organic molecular moieties, resulting in a burly SEI on the anode, thus irreversible reduction (decomposition) of the electrolyte solvents could be restrain. On the other hand, transition metal ions could combine with decomposition products such as $RSO_3^-$, $ROSO_3^-$ and $SO_3^{2-}$ anions to form insoluble transition metal sulfates or sulfites, resulting in a dense and thick CEI, which will reduce dissolution of transition metal ions (Fig. 7c).

Generally, Ni–Fe-Mn-based materials exhibit good cycling performance, but significant performance deterioration along with structure monoclinic distortion often occur in the high voltage region (> 4.0 V), while the plateau voltage needs to be increased to obtain higher energy density for practical applications. In addition, dissolution of transition metal ions and side reactions between active materials and electrolytes occurs during cycles, leading to loss and fracture of active material. For the above problems, ion doping, surface modification and composite structure construction are effective strategies.

#### *1.1.6 Ion doping*

The ion doping can modulate the crystal structure and make the phase transition highly reversible, while the dopant ions can combine with oxygen ions to form stronger chemical bonds, increasing the solidity of the layered structure. The Ti instead of Mn not only increases the lattice spacing, but also can lift the working potentials [69], which delivered improved cyclic performance (capacity retention of 84% after 200 cycles at 0.1C) and higher energy density of about 460 Wh $kg^{-1}$. Ding and co-workers [138] realized atomic-level mixing of Ti in Ni–Fe-Mn based materials by sol–gel method. The $Na[Ni_{0.4}Mn_{0.4}Fe_{0.2}]_{0.95}Ti_{0.05}O_2$ showed excellent rate capacities of 160.7, 132.1, 125.1, 120.9, 114.7 and 99.6 mAh $g^{-1}$ at 0.1, 0.2, 0.5, 1.0, 2.0 and 5.0 C at 2.0–4.0 V, respectively (1C = 140 mA $g^{-1}$) due to the larger parameter c from Ti introduction. The corresponding capacity retention also increased from 69.6% ($NaNi_{0.4}Mn_{0.4}Fe_{0.2}O_2$) to 83.8% after 200 cycles at 1 C. In addition, it is verified that the irreversible multiphase transformation of the P3 to O3 phase was effectively restrained. Recently, Park [139] confirmed the energy barrier of $Na^+$ migration decreased after Ti substitution into O3-type $NaFe_{0.25}Ni_{0.25}Mn_{0.5}O_2$ based on DFT calculations.

The main factors limiting the performance of O3 Ni–Fe-Mn based layered oxide materials are migration of transition metal ions and irreversible phase change at high voltage. The transition metal ions in TM layer migrate to adjacent Na layer, hindering the transport of sodium ions. In a high cut-off voltage (> 4 V), with most $Na^+$ extracting from the unit cell, the layer structure tends to glide and distort, leading irreversible phase transformation, which is accompanied by large variation of the lattice volume and a fast capacity attenuation. Sun [140] proposed Li introduction into the transition metal

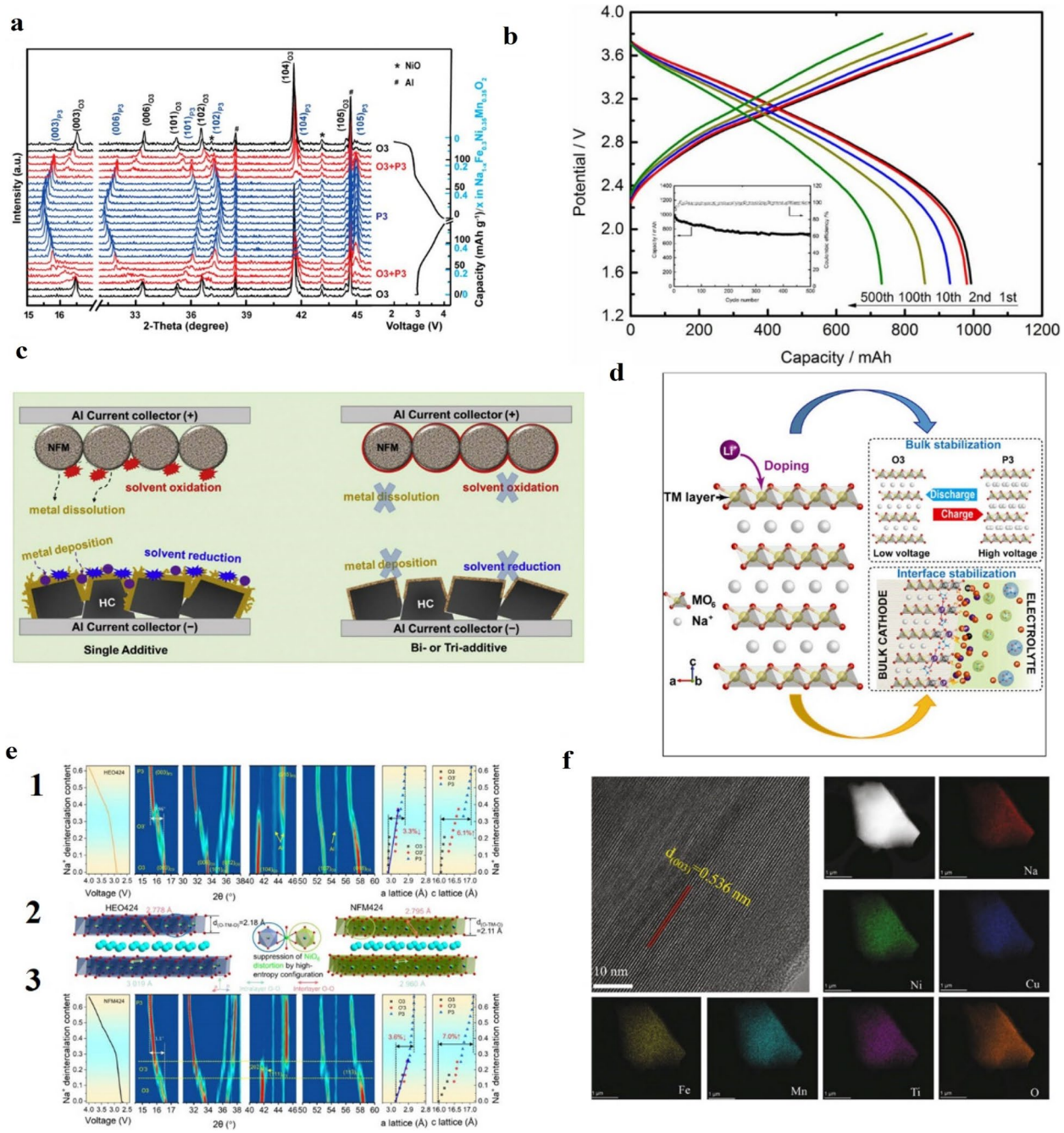


**Fig. 7** **a** In situ XRD patterns of $NaFe_{0.3}Ni_{0.35}Mn_{0.35}O_2$ tested within 2.0 − 4.0 V, in which the black and blue scales (right) represent capacity and corresponding x value in $Na_{1-x}Fe_{0.3}Ni_{0.35}Mn_{0.35}O_2$, respectively. Reproduced with permission [68]. Copyright 2019, American Chemical Society. **b** The voltage profiles of a 1 Ah soft-packed sodium ion battery cycled between 1.5 V and 3.8 V at 1 C rate. Reproduced with permission [27]. Copyright 2019, Electrochemical Society, Inc. **c** Schematic summary on the role of PST and DTD additives in HC/NFM full cell. Reproduced with permission. [28] Copyright 2018, Elsevier B.V. **d** Dual-stabilization effect of the cation dopants on the evolution of bulk structure and electrode–electrolyte interphase of a Li-substituted O3-type cathode. Reproduced with permission [70]. Copyright 2018, Cell Press. **e** Structural evolution during the initial charge process. 2D contour plots of in situ XRD during the structural evolution of HEO424 $e_1$ and NFM424 $e_3$ cathodes. $e_2$ Schematic illustrations showing the TMO2 slabs in both cathodes. The first charge curves as a function of $Na^+$ deintercalation content are plotted on the right, and the a/c-axis lattice parameter changes in the as-prepared samples obtained by fitting the in situ XRD data are plotted on the left. Reproduced with permission [72]. Copyright 2022, American Chemical Society. **f** HRTEM image and EDS mapping of NNCFMTO sample. Reproduced with permission [73]. Copyright 2021, Elsevier B.V

layer could remain structure stability due to stronger Li−O bond relative to Ni−O and Mn−O bonds and the migration of $Fe^{3+}$ could be restrain. In addition, electronic conductivity, capacity, its retention, and rate capability were improved after Li incorporation. Guo [70] put forward the dual-stabilization effect of Li substitution in high-voltage in detail. One is unfavorable P3-P'3 phase transition at high voltages (> 4.2 V) was suppressed due to the weak Jahn–Teller distortion of $Ni^{3+}$. The other is Li may bond with $F^-$ anion, leading a stable electrolyte-cathode interphase, which is useful for less transition metal ions dissolution (Fig. 7d). Thus, the Li doped sample $Na_{0.85}Li_{0.1}Ni_{0.175}Mn_{0.525}Fe_{0.2}O_2$ displayed a high discharge capacity of 160 mAh $g^{-1}$ at 0.1 C at the voltage of 2.0–4.5 V and excellent capacity of 88% after 100 cycles at 1 C. It is well-established that $Mn^{3+}$ ions are accompanied by strong Jahn–Teller effect, which seriously damage the structural stability and the cyclic performance. By suitable element doping, the content of $Mn^{3+}$ can be reduced and thus the structural stability can be improved. Liu [141] prepared O3-$NaMn_{0.48}Ni_{0.2}Fe_{0.3}Mg_{0.02}O_2$ materials, which showed lower $Mn^{3+}$ and minimize Jahn−Teller effect, leading outstanding structure stability. The reversible capacity almost has no attenuation after 100 cycles at 0.1 C in the voltage range of 1.5–4.2 V (the capacity retention of $NaMn_{0.5}Ni_{0.2}Fe_{0.3}O_2$ is 81%). Huang [71] proposed that F-doped result in a lower $Mn^{3+}$ content, which stabilize the O3-type layered structure. However, the discharge capacity has little decrease. So, it is crucial to have balance for cyclic performance and reversible capacity. In addition to the elements mentioned above, Ca [142], Al [143] and Zn [144] were proved to have remarkable enhancement on rate capability, cycling stability and reversible phase transformation.

Co-doping of multiple elements are an effective strategy to obtain a sample with excellent overall performance, such as high thermal stability and fracture toughness, splendid low temperature performance, high strength and air stability [145–147]. In the layered oxide cathode, $Ni^{2+}$, $Fe^{3+}$ and $Cu^{2+}$ could provide charge compensation for high capacity delivery, $Mg^{2+}$, $Mn^{4+}$ and $Ti^{4+}$ have positive effect on structure stability, $Sn^{4+}$ and $Sb^{5+}$ could raise the average voltages of the materials, which increase energy density. $Co^{3+}$ has electrochemical activity and may counter the Jahn−Teller effect of $Mn^{3+}$, leading to good structure stability. Hu's and co-workers [72] employed high-entropy configuration strategy to design O3-type $NaNi_{0.25}Mg_{0.05}Cu_{0.1}Fe_{0.2}Mn_{0.2}Ti_{0.1}Sn_{0.1}O_2$ oxide. It was proposed that the multicomponent transition metal ions strengthen the whole skeleton structure of layered oxides by weaker Jahn−Teller distortion, $Na^+$/vacancy ordering, and lattice parameter changes (Fig. 7e). Meanwhile, the $TMO_2$ slabs were expanded to make sure faster ion transport, compared to the baseline sample ($NaNi_{0.4}Fe_{0.2}Mn_{0.2}O_2$). This material delivered a reversible capacity of about 130.8 mAh $g^{-1}$ and energy density of 421 Wh $Kg^{-1}$ in a voltage range of 2.0–4.0 V at 0.1 C (1 C = 140 mA $g^{-1}$). It remained a capacity retention of 75% over 500 cycles at 1 C, which is much higher than the baseline sample (38%). It also showed outstanding full cell performance when coupled with hard carbon as anode. The discharge capacity and energy density reached 123.5 mAh $g^{-1}$ (based on cathode mass) and 260 Wh $kg^{-1}$ (based on the total mass of active materials) in the voltage range of 1.0–4.0 V at 0.1 C. The capacity retention is about 76.5% after 500 cycles at 0.5 C, which is pretty outstanding compared to the other layered oxide cathode. Chen and co-workers [73] designed a five-components O3-type layered oxide cathode ($Na_{0.94}Ni_{0.29}Cu_{0.1}Fe_{0.16}Mn_{0.3}Ti_{0.15}O_2$) with uniform distribution of elements (Fig. 7f). The charge–discharge curve is consisted of voltage plateau around 3 V and a sloping voltage profile at 3.0–4.0 V, which is corresponding to a highly reversible O3-P3 phase transition (without any monoclinic phase). So, it delivered a reversible capacity of 122 mAh $g^{-1}$ and high capacity retention of more than 79% after 300 cycles at 0.5 C in the voltage of 2.0–4.0 V. Recently, Lin et al. [148]. also reported a high-entropy O3-type cathode, containing similar chemical composition. The $NaCu_{0.1}Ni_{0.3}Fe_{0.2}Mn_{0.2}Ti_{0.2}O_2$ showed excellent long-term cycling stability (approximately 71% after 500 cycles at 0.5 C), which is attributed to the stabilization effect of entropy [149, 150].

In short, ion doping is an effective strategy to suppress irreversible phase transitions, reduce transition metal ion dissolution and improve the structural stability of layered materials. However, the mechanism of ion doping for material property improvement still needs further exploration and in-depth study, especially multi-ion co-doping.

#### *1.1.7 Surface modification*

In addition to the ion doping, surface modification is also one of the effective strategies to enhance overall performance of cathode. Uniform coating layer can mitigate the corrosion of cathode from the electrolyte and maintain structural integrity, resulting an improved long cycle performance. In particular, the fast ion conductor such as $NaTi_2(PO_4)_3$ [151, 152], $Na_2SiO_3$ [74] and etc. as coating layer can accelerate $Na^+$ diffusion at the interface, further increasing the rate performance. Xiao and co-workers [74] reported a O3 $NaNi_{1/3}Mn_{1/3}Fe_{1/3}O_2$ uniformly wrapped by Na-ion conductor $Na_2SiO_3$ via in situ coating (Fig. 8a). The $Na_2SiO_3$ coating layer can reduce polarization and suppress voltage drop during charge–discharge process. Meanwhile, $Na^+$ diffusion

was effectively improved due to the three-dimensional structure of $Na_2SiO_3$. Thus, 5 mol% $Na_2SiO_3$ coated $NaNi_{1/3}Mn_{1/3}Fe_{1/3}O_2$ cathode showed excellent cycling performance. The capacity retention could reach 88.3% after 200 cycles at 0.5 C in the voltage of 1.5–4.2 V. The rate capacity is 58 mAh $g^{-1}$ at current density of 5 C, while the uncoated sample remain a capacity of only 12 mAh $g^{-1}$. Yu et al. [36] reported a synergetic strategy to improve electrochemical performance of Ni–Fe-Mn based cathode by integration $TiO_2$ coating and $Ti^{4+}$ doping. On the one hand, the $TiO_2$ coating on the surface of the particle inhibits the side reaction and reduces the dissolution of transition metal ions. On the other hand, $Ti^{4+}$ is successfully doped into transition metal layer of bulk phase structure, while increases the sodium layer spacing and improves the diffusion of sodium ions. In addition, the content of $Mn^{3+}$ is reduced and the Jahn – Teller effect is suppressed, leading entirely reversible phase transformation (Fig. 8b). This material yields fabulous rate capability of 197.2, 160.9, 140.7, 118.3, 103.6, 88.3, 62.6, 41.8, and 30.0 mAh $g^{-1}$ at 0.05, 0.1, 0.2, 0.5, 1, 2, 5, 8, and 10 C (1 C = 200 mA $g^{-1}$), respectively. It also delivered good cycling stability with about 56.2% and 71.0% at 0.1 and 1 C after 100 cycles in the voltage of 1.5–4.2 V. As we all know that oxygen ions may participate in redox to provide additional capacity, which is common in the cathode materials for Li-ion batteries. Liu and co-workers [75] adopt similar synergetic strategy to enhance the rate and cyclic performance by simultaneously coating and doping. In particular, $Zr^{4+}$ doping adjusts the Na–O-TM structure and the electronic state of O-2p occupies a higher energy level which is supported by DFT calculations, resulting in the higher reversibility and cycle stability of oxygen redox (Fig. 8c). Thus, $ZrO_2$ coated $NaNi_{1/3}Fe_{1/3}Mn_{1/3}O_2$ delivered high reversible specific capacity of 152.4 and 157.1 mAh $g^{-1}$ at 0.05 C in the voltage of 1.5–4.3 and 1.5–4.6 V, respectively. It also remains a capacity retention of 81.9% at 100 cycles at 1 C.

Air stability has a huge impact on electrode assembly, production and transportation. Uniform and dense coating layer can solve this problem very well. Lamb et al. [100]. reported a phosphate-based coating on O3 $Na(Ni_{0.3}Fe_{0.4}Mn_{0.3})O_2$. The capacity retention of 1% $(NaPO_3)_n$ coating $Na(Ni_{0.3}Fe_{0.4}Mn_{0.3})O_2$ increased 14.0% after 100 cycles at 0.25 C, compared to the pristine $Na(Ni_{0.3}Fe_{0.4}Mn_{0.3})O_2$ (Fig. 8d). After exposed to the ambient air for 9 days, it only loss a capacity of 30 mAh $g^{-1}$ (the capacity loss of pristine sample is 80 mAh $g^{-1}$). The reasons for showing excellent cyclic performance and air stability could be attributed to the following points: firstly, the coating layer reduced corrosion of electrode materials by electrolyte. Secondly, when a large quantity of phosphate coating is applied, sodium is leached from the bulk to form sodium phosphate, leading to the formation of inert metal oxides on the surface. It is worth pointing out that over 1 wt% coating will cause lower initial capacity. In addition, some other materials such as $Al_2O_3$ [153] and $AlF_3$ [45] were also employed as effective coating layer to improve structure stability and integrality. A portion of the coating material will cause a slight decrease in reversible capacity and energy density, so proper addition ratio is critical.

### 1.2 Composite structure construction

Many mixing P/O phases have been synthesized to improve cycling and rate performance depending on synergistic effects of multiple phases. As we all know, Although O3 materials have a high capacity, O3-type materials usually require more diffusion energy barrier through intermediate tetrahedral sites during sodium ion extraction/insertion, and thus are accompanied by unsatisfactory rate performance and cycling stability. Integrating P-type phase into O3-type materials at the microscale can adequately take advantage of the high stability of P-type materials and high capacity of O-type materials.

Passerini and co-workers [154] prepared a quaternary P3/P2/O3-type layered cathode ($Na_{0.76}Mn_{0.5}Ni_{0.3}Fe_{0.1}Mg_{0.1}O_2$) (Fig. 9a), which showed high reversible capacity, average coulombic efficiencies and excellent capacity retention. It is mainly due to the synergetic effect on the electrochemical performance from mixed phase. The O3 phase make sure a high reversible capacity as a result of higher sodium content; The P2 and P3 phases supply outstanding rate capacity and cyclic performance depending on the P-type structure (lower $Na^+$ migration energy barrier via prismatic sites); Furthermore, the O-type and P-type phases may have inverse c-axis parameters changes, further decreasing strain inside the electrode. This material delivered a high initial reversible capacity of 155 mAh $g^{-1}$ with average coulombic efficiencies of over 99% as well as a capacity retention of 90.2%

(See figure on next page.)

**Fig. 8** **a** $a_1$ The structure of $Na_2SiO_3$. $a_2$ Schematic illustration of the synthesis process for $Na_2SiO_3$@$NaNi_{1/3}Mn_{1/3}Fe_{1/3}O_2$. Reproduced with permission [74]. Copyright 2019, Elsevier B.V. **b** In situ XRD patterns of $TiO_2$@MFN during the charge – discharge process. Reproduced with permission [36]. Copyright 2020, American Chemical Society. **c** $c_1$ Na–O-TM structure before and after $Zr^{4+}$ doping. $c_2$ $Mn^{4+}$, $Fe^{3+}$, $Ni^{2+}$ and $O^{2-}$ electronic states of the outermost orbit. DOS schematic diagrams of $c_3$ MFN and $c_4$ $ZrO_2$@MFN. Reproduced with permission [75]. Copyright 2021, Elsevier B.V. **d** $d_1$ Illustrated diagram of the ammonium dihydrogen phosphate (top) and phosphoric acid (bottom) coating methods. $d_2$ Cycling performance of uncoated and coated NFM at a C/5 rate. Reproduced with permission [100]. Copyright 2021, American Chemical Society

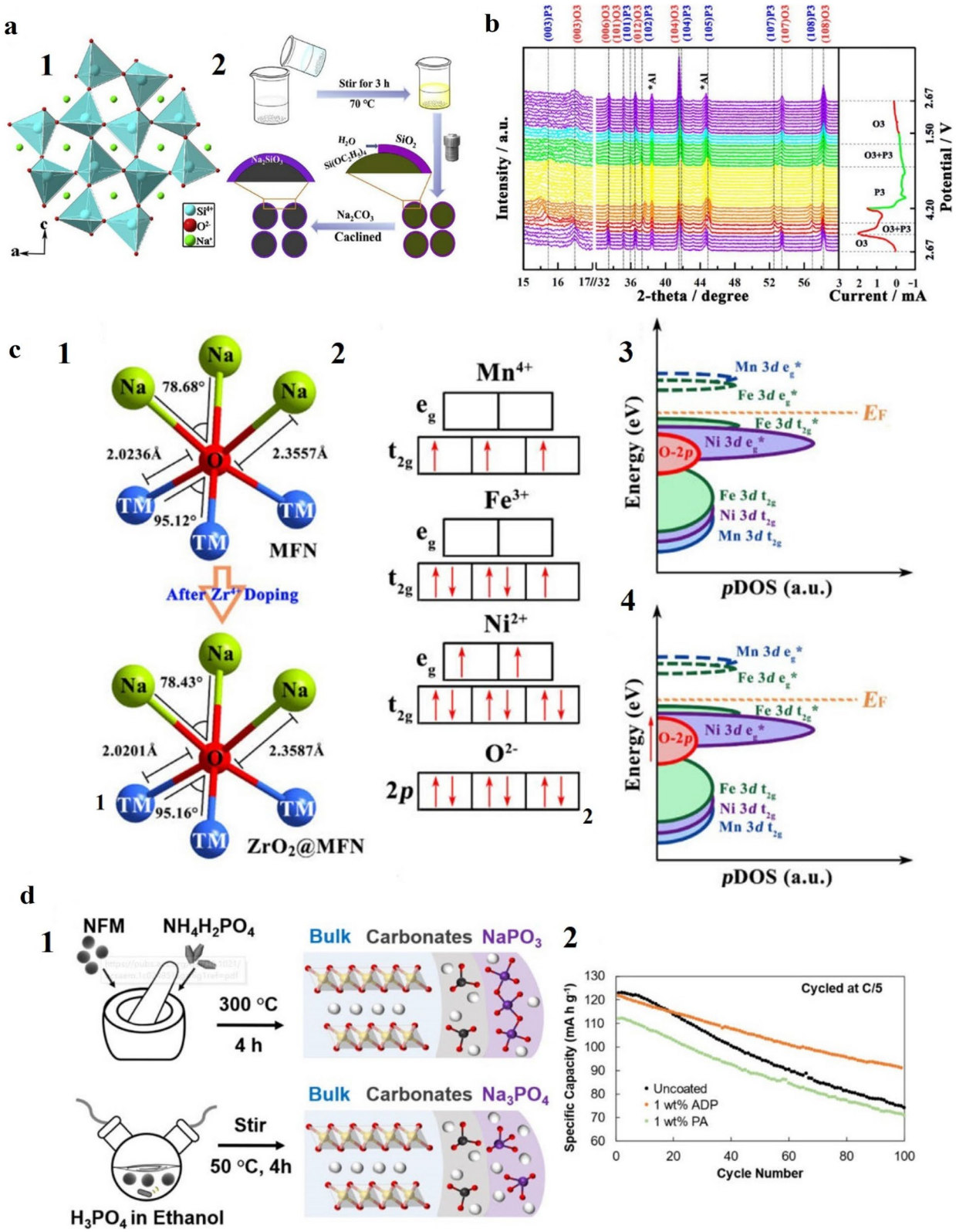


**Fig. 8** (See legend on previous page.)

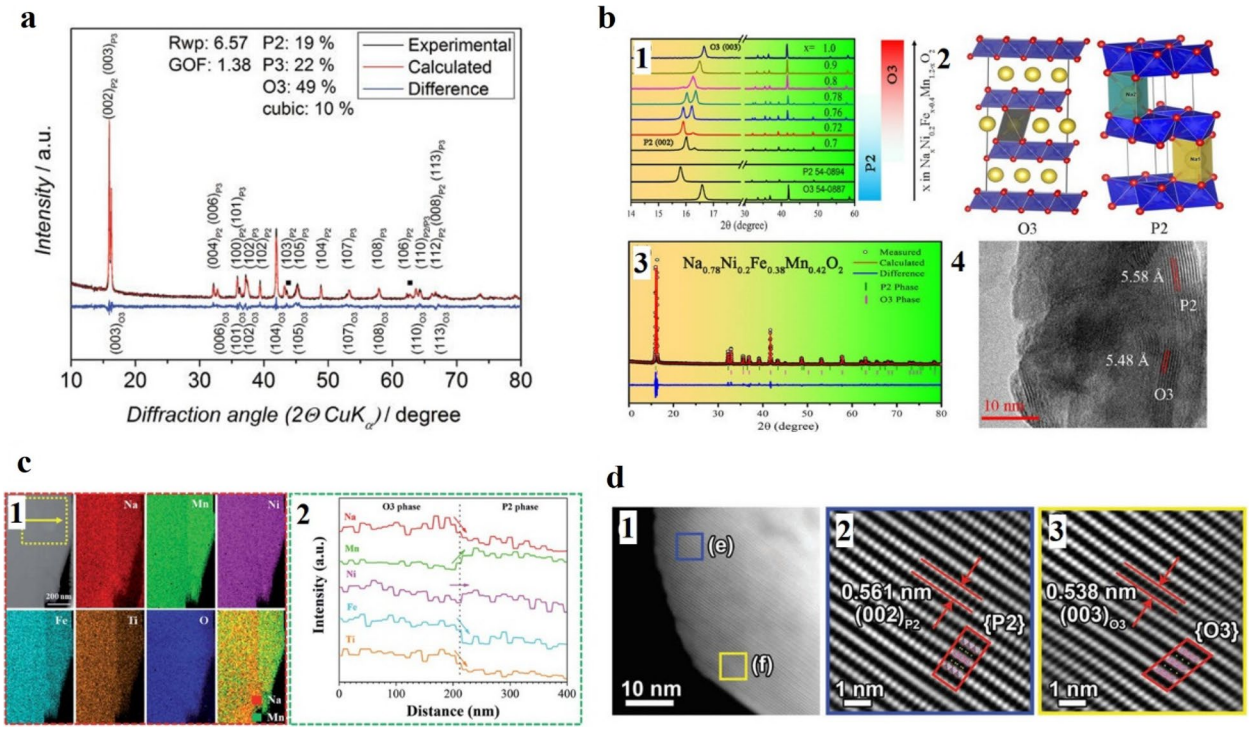


**Fig. 9** **a** X-ray diffraction pattern and Rietveld refinement of P3/P2/O3-material (cubic $Mg_{1-x}Ni_xO$ (x≈0.3) phase is marked with squares). Reproduced with permission [154]. Copyright 2016, Wiley–VCH. **b** $b_1$ X-ray diffraction patterns of $Na_xNi_{0.2}Fe_{x-0.4}Mn_{1.2-x}O_2$ with different Na contents (0.7 – 1.0) and the phase evolution derived from XRD patterns is shown in the right. $b_2$ Schematic illustration of O3 (left) and P2 (right) structures. $b_3$ Observed and calculated XRD profiles for NNFM-0.78 with $b_4$ TEM image of this material. Reproduced with permission [40]. Copyright 2017, American Chemical Society. **c** $c_1$ STEM-EDX HAADF image and elemental distribution maps; $c_2$ line profile representing the elemental intensities averaged over 360 nm parallel to the interface. Reproduced with permission [155]. Copyright 2021, Royal Society of Chemistry. **d** $d_1$-$d_3$ HRTEM images of the biphasic domain of NMFML. Reproduced with permission [76]. Copyright 2022, Wiley–VCH

after 601 cycles at 1 C in the voltage range of 2.5–4.3 V. Chen and co-workers [40] synthesized a O3/P2 mixed phases cathode via adjustment of sodium content (Fig. 9b). The $Na_{0.78}Ni_{0.2}Fe_{0.38}Mn_{0.42}O_2$ cathode delivered a capacity of 86 mAh $g^{-1}$ and capacity retention of 90% after 1500 cycles at 10 C in the voltage range of 2.5–4.0 V. On the first charge/discharge, the O3 phase undergone a highly reversible O3–P3-O"3–P3–O3 sequence phase transformation and the P2 phase almost have no change. However, when the upper voltage increases to 4.3 V, the P2 phase transform to Z phase along with the reduction of P2 (002) peak intensity, indicating the structure may be damaged. It is necessary to enhance structure stability in the high voltage region. Wang et al. [155] prepared a series of P/O intergrown biphasic $Na_{0.8}Mn_yNi_{0.8-y}Fe_{0.1}Ti_{0.1}O_2$ (y = 0.6, 0.55, 0.5, 0.45) layered cathode. Among them $Na_{0.8}Mn_{0.55}Ni_{0.25}Fe_{0.1}Ti_{0.1}O_2$ showed a superior reversible of 154.6 mAh $g^{-1}$ with satisfying initial coulombic efficiency (~ 100%) as well as high capacity retention of 80.2% after 100 cycles at 0.1C in the voltage range of 1.5–4.3 V. The P/O phases intergrowth in a single particle with a semi-coherent interface along the c and a/b axes is observed directly by TEM characterization (Fig. 9c). Sun et al. [76] presented a novel P2/O3 biphasic $Na_{7/9}Ni_{2/9}Mn_{4/9}Fe_{1/9}Mg_{1/9}Li_{1/9}O_2$ cathode. The topotactic intergrown structure suppressed deleterious phase transformations in the high-voltage region and alleviated internal stress (Fig. 9d). In addition, low oxidation state dopants suppress the dissolution of active materials owing to the charge-compensation mechanism. The materials showed an excellent electrochemical performance, thermal stability and air stability. It delivers a discharge capacity of 170.5 mAh $g^{-1}$ at 0.1 C and outstanding capacity retention of 71.8% after 500 cycles at 5 C in voltage range of 2.0–4.4 V. The full cell of $Na_{7/9}Ni_{2/9}Mn_{4/9}Fe_{1/9}Mg_{1/9}Li_{1/9}O_2$/hard carbon could deliver a high energy density of 282.6 W h $kg^{-1}$ with an operating potential of ≈3.2 V, indicating its practical viability.

Mixed-phase materials exhibit excellent electrochemical properties, but their synthesis conditions are complex and require precise tuning of elemental composition, which is very challenging. In addition, the interface of

the two phases and the elemental composition through the interface are unclear, and the phase transition mechanism of the multiphase still needs further investigation.

## 2 Conclusion and perspectives

In summary, we have comprehensively reviewed the recent progress, key challenges and solutions of O3-type $Na_xNi_yFe_zMn_{1-y-z}O_2$ layered oxide cathodes. The key challenges mainly contained irreversible phase transitions, highly hygroscopic and insufficient cell performance.

(i) Irreversible phase transition: Usually, O3-type materials are accompanied by multi-level irreversible phase changes during the desodiation process, and the large volume changes will trigger the nonuniform accumulation of stress, which eventually lead to microcracks or even fragmentation of the material particles, resulting in more electrolyte attack and a significant decrease in cycling performance. Since irreversible phase transitions easily lead to structural collapse and a rapid capacity degradation, suppressing or reducing these irreversible phase transitions is key to improving the electrochemical performance of layered oxides.
(ii) Highly hygroscopic: Another challenge is the inherent hygroscopic properties of the O3-type material when exposed to ambient air. On the one hand, $H_2O$ embedded in the material forms a hydrated phase, which may prevent the transfer of $Na^+$; on the other hand, it has been shown that the material undergoes spontaneous exchange of $Na^+$ and $H^+$, leading to the loss of bulk $Na^+$ and the aggregation of surface Na (electrochemically inactive NaOH or $Na_2CO_3$), which increases the alkalinity of the material and the impedance during cycle. In addition, it may trigger the gelation of the slurry, increasing production difficulties and storage costs. Therefore, it is crucial to improve the air stability in order to further scale up the material.
(iii) Insufficient cell performance: Considering the cost advantage of sodium ion batteries, Fe and Mn elements are crucial; however, Fe elements may migrate to the tetrahedral sites of the alkali metal layer during charge and discharge process, hindering $Na^+$ transport and causing performance degradation. Meanwhile, the Jahn–Teller effect of $Mn^{3+}$ will cause lattice distortion and increase the irreversibility of the phase transition, therefore, the valence state of Mn needs to be increased. Thus, migration of transition metal ions and Jahn–Teller effect need to be improved by proper structure design due to the decisive influence for cyclic stability.

Possible solutions are suggested as follows:

(i) The ion doping can mitigate irreversible phase transitions and have a "pinning" effect on structure stability, such as Ti,Mg. Ti doping can significantly smooth voltage curves and increases energy density, effectively suppressing irreversible phase transitions. Mg doping suppress slippage of the transition metal layer, leading enhanced cycling stability in the high voltage region.
(ii) The improvement of hygroscopicity can be achieved in two ways, one is doping with elements that can improve water-resistant property, such as Cu, Mg and so on. On the other hand, the surface coating layer can reduce the contact between the bulk phase and the air, therefore leading to the enhanced air stability. In addition, surface coating layer also decrease electrolyte attack and reduce the dissolution of transition metal ions.
(iii) The migration of transition metal ions can be improved by doping with elements that can act as pillar ions (such as Zn, Zr), while reducing the content of elements is also an effective way. the Jahn–Teller effect of Mn can be reduced by reducing the content of $Mn^{3+}$.

In order to achieve the commercialization process of sodium ion batteries, the air stability and cyclic performance of the O3-type cathode material is crucial, elemental doping followed by surface coating is recommended. High entropy materials with the advantage of multiple elements synergistic effect brings excellent properties, such as high fracture toughness, high strength and good long cyclic properties. However, they are generally synthesized by the one step high temperature solid-state method (direct mixing of oxides), resulting in slightly lower tap density and energy density compared with secondary spherical particles of Li-NiCoMn materials system. Therefore, the synthesis of high-entropy cathode materials with secondary spherical morphology will be very promising.

Most studies focus on half-cell based on sodium as the anode. However, it is known that full cell usually chooses disordered carbons, mainly hard carbons (HCs) as the anode due to the potential safety risks of sodium. It will have different performance delivery compared with half cells. Continuous work on electrolyte additives, separators and proper anode materials is also needed to further promote the practical application of Na full cell. Several companies and teams have already performed the preparation of full cells, soft packs and cylindrical cells, and gradually brought them to the market. Sodium ion batteries based on O3-type cathode materials show great

market prospects for applications in electric bicycle, low-speed electric vehicles and large-scale energy storage applications. It can be anticipated that advanced electrode material with outstanding electrochemical performance, cost efficiency, and environmental friendliness are emerging, and will eventually contribute to the practical energy storage market in the near future.

**Abbreviations**

| | |
|---|---|
| EV | Electric vehicles |
| HEV | Hybrid electric vehicles |
| NIBs | Sodium-ion batteries |
| ICEL | initial coulombic efficiency |
| DFT | Density functional theory |
| ALD | Atomic layer deposition |
| PVDF | Polyvinylidene fluoride |
| HCs | Hard carbons |

**Acknowledgements**
Not applicable.

**Authors' contributions**
SZ: organized the framework of the manuscript, drafted, and revised the manuscript. QS, WF, YL, XY, XZ, XL: gave some comments and suggestion. YZ: modified the manuscript. All authors have read and agreed to this version of manuscript.

**Funding**
Open access funding provided by Shanghai Jiao Tong University. This work is supported by the National Natural Science Foundation of China (22179077, 51774251, 21908142), Shanghai Science and Technology Commission's "2020 Science and Technology In-novation Action Plan" (20511104003), Natural Science Foundation in Shanghai (21ZR1424200).

**Availability of data and materials**
The data involved in the manuscript can be found in the references which are listed at the end of the paper.

## Declarations

**Ethics approval and consent to participate**
All authors have seen the manuscript and approved to submit to the journal.

**Consent for publication**
This manuscript has not been published in whole or in part nor is it being considered for publication elsewhere.

**Competing interests**
There are no financial interests that are directly or indirectly related to the work submitted for publication.

Received: 5 April 2023 Revised: 29 May 2023 Accepted: 13 June 2023
Published online: 29 June 2023

**References**

1. Kubota K, Kumakura S, Yoda Y, Kuroki K, Komaba S (2018) Electrochemistry and solid-state chemistry of $NaMeO_2$ (Me = 3d transition metals). Adv Energy Mater 8:1703415. https://doi.org/10.1002/aenm.201703415
2. Hwang JY, Myung ST, Sun YK (2017) Sodium-ion batteries: present and future. Chem Soc Rev 46:3529–3614. https://doi.org/10.1039/c6cs00776g
3. Ren H, Li Y, Ni Q, Bai Y, Zhao H, Wu C (2022) Unraveling anionic redox for sodium layered oxide cathodes: breakthroughs and perspectives. Adv Mater 34:2106171. https://doi.org/10.1002/adma.202106171
4. Huang Z-X, Zhang X-L, Zhao X-X, Heng Y-L, Wang T, Geng H, Wu X-L (2022) Hollow $Na_{0.62}K_{0.05}Mn_{0.7}Ni_{0.2}Co_{0.1}O_2$ polyhedra with exposed stable {001} facets and K riveting for sodium-ion batteries, Sci. China. Mater 66;79–87. https://doi.org/10.1007/s40843-022-2157-8.
5. Li J-Q, Yang Y-J, Pang J (2015) Electrochemical and structural performances of $Li[N_{i0.133}Li_{0.2}Co_{0.133}Mn_{0.533}]O_2$ material during different cycle potential windows, Rare Metals 41;2664–2670. https://doi.org/10.1007/s12598-015-0562-x.
6. Goikolea E, Palomares V, Wang S, Larramendi IR, Guo X, Wang GX, Rojo T (2020) Na-ion batteries—approaching old and new challenges. Adv Energy Mater 10:2002055. https://doi.org/10.1002/aenm.202002055
7. Xiao Y, Abbasi NM, Zhu YF, Li S, Tan SJ, Ling W, Peng L, Yang TQ, Wang L, Guo XD, Yin YX, Zhang H, Guo YG (2020) Layered oxide cathodes promoted by structure modulation technology for sodium-ion batteries. Adv Funct Mater 30:2001334. https://doi.org/10.1002/adfm.202001334
8. Zuo W, Qiu J, Liu X, Ren F, Liu H, He H, Luo C, Li J, Ortiz GF, Duan H, Liu J, Wang MS, Li Y, Fu R, Yang Y (2020) The stability of P2-layered sodium transition metal oxides in ambient atmospheres. Nat Commun 11:3544. https://doi.org/10.1038/s41467-020-17290-6
9. Wang Y, Zhao X, Jin J, Shen Q, Zhang N, Qu X, Liu Y, Jiao L (2022) Low-cost layered oxide cathode involving cationic and anionic redox with a complete solid-solution sodium-storage behavior. Energy Storage Mater 47:44–50. https://doi.org/10.1016/j.ensm.2022.01.047
10. Yuan XG, Guo YJ, Gan L, Yang XA, He WH, Zhang XS, Yin YX, Xin S, Yao HR, Huang Z, Guo YG (2022) A universal strategy toward air-stable and high-rate O3 layered oxide cathodes for Na-Ion batteries. Adv Funct Mater 32:2111466. https://doi.org/10.1002/adfm.202111466
11. Yao HR, Wang PF, Gong Y, Zhang J, Yu X, Gu L, OuYang C, Yin YX, Hu E, Yang XQ, Stavitski E, Guo YG, Wan LJ (2017) Designing air-stable O3-type cathode materials by combined structure modulation for Na-Ion Batteries. J Am Chem Soc 139:8440–8443. https://doi.org/10.1021/jacs.7b05176
12. Yu TY, Ryu HH, Han G, Sun YK (2020) Understanding the capacity fading mechanisms of O3-Type $Na[Ni_{0.5}Mn_{0.5}]O_2$ cathode for sodium-Ion batteries, Adv. Energy Mater 10;2001609. https://doi.org/10.1002/aenm.202001609.
13. Huang Z-X, Gu Z-Y, Heng Y-L, Huixiang Ang E, Geng H-B, Wu X-L (2023) Advanced layered oxide cathodes for sodium/potassium-ion batteries: development, challenges and prospects, Chem Eng J 452;139438. https://doi.org/10.1016/j.cej.2022.139438.
14. Kim H, Shakoor RA, Park C, Lim SY, Kim J-S, Jo YN, Cho W, Miyasaka K, Kahraman R, Jung Y, Choi JW (2013) $Na_2FeP_2O_7$ as a promising iron-based pyrophosphate cathode for sodium rechargeable batteries: a combined experimental and theoretical study. Adv Funct Mater 23:1147–1155. https://doi.org/10.1002/adfm.201201589
15. Ren L, Song L, Guo Y, Wu Y, Lian J, Zhou Y-N, Yuan W, Yan Q, Wang Q, Ma S, Ye X, Ye Z, Lu J (2021) Magnesium-doped $Na_2FeP_2O_7$ cathode materials for sodium-ion battery with enhanced cycling stability and rate capability, Appl Surf Sci 544;148893. https://doi.org/10.1016/j.apsusc.2020.148893.
16. Chen M, Chen L, Hu Z, Liu Q, Zhang B, Hu Y, Gu Q, Wang JL, Wang LZ, Guo X, Chou SL, Dou SX (2017) Carbon-coated $Na_{3.32}Fe_{2.34}(P_2O_7)_2$ cathode material for high-rate and long-life sodium-ion batteries, Adv Mater. 29;1605538. https://doi.org/10.1002/adma.201605535.
17. Yuan TC, Wang YX, Zhang JX, Pu XJ, Ai XP, Chen ZX, Yang HX, Cao YL (2019) 3D graphene decorated $Na_4Fe_3(PO_4)_2(P_2O_7)$ microspheres as low-cost and high-performance cathode materials for sodium-ion batteries. Nano Energy 56:160–168. https://doi.org/10.1016/j.nanoen.2018.11.011
18. Qian JF, Wu C, Cao YL, Ma ZF, Huang YH, Ai XP, Yang HX (2018) Prussian blue cathode materials for sodium-ion batteries and other ion batteries. Adv Energy Mater 8:1702619. https://doi.org/10.1002/aenm.201702619
19. Wang W, Gang Y, Hu Z, Yan Z, Li W, Li Y, Gu QF, Wang Z, Chou SL, Liu HK, Dou SX (2020) Reversible structural evolution of sodium-rich rhombohedral prussian blue for sodium-ion batteries. Nat Commun 11:980. https://doi.org/10.1038/s41467-020-14444-4
20. Yang DZ, Liao XZ, Huang BW, Shen J, He YS, Ma ZF (2013) A $Na_4Fe(CN)_6$/NaCl solid solution cathode material with an enhanced electrochemical

performance for sodium ion batteries. J Mater Chem A 1:13417–13421. https://doi.org/10.1039/c3ta12994b
21. Wang P-F, You Y, Yin Y-X, Guo Y-G (2018) Layered oxide cathodes for sodium-ion batteries: phase transition, air stability, and performance. Adv Energy Mater 8:1701912. https://doi.org/10.1002/aenm.201701912
22. Wang S, Sun C, Wang N, Zhang Q (2019) Ni- and/or Mn-based layered transition metal oxides as cathode materials for sodium ion batteries: status, challenges and countermeasures. J Mater Chem A 7:10138–10158. https://doi.org/10.1039/c8ta12441h
23. Deng J, Luo W-B, Chou S-L, Liu H-K, Dou S-X (2018) Sodium-Ion batteries: from academic research to practical commercialization. Adv Energy Mater 8:1701428. https://doi.org/10.1002/aenm.201701428
24. Wei F, Zhang Q, Zhang P, Tian W, Dai K, Zhang L, Mao J, Shao G (2021) Review—research progress on layered transition metal oxide cathode materials for sodium Ion batteries, J. Electrochem Soc 168;050524. https://doi.org/10.1149/1945-7111/abf9bf.
25. Zhao CL, Lu YX, Chen LQ, Hu YS (2019) Ni-based cathode materials for Na-ion batteries. Nano Res 12:2018–2030. https://doi.org/10.1007/s12274-019-2451-3
26. Rong X, LU Y, Qi X, Zhou Q, Kong W, Tang K, Chen L, Hu Y (2020) Na-ion batteries: from fundamental research to engineering exploration, Energy Storage Science and Technology 9;516–521. https://doi.org/10.19799/j.cnki.2095-4239.2020.0054.
27. Wang H, Liao XZ, Yang Y, Yan XM, He YS, Ma ZF (2016) Large-scale synthesis of $NaNi_{1/3}Fe_{1/3}Mn_{1/3}O_2$ as high performance cathode materials for sodium ion batteries. J Electrochem Soc 163:A565–A570. https://doi.org/10.1149/2.0011605jes
28. Che H, Yang X, Wang H, Liao X-Z, Zhang SS, Wang C, Ma Z-F (2018) Long cycle life of sodium-ion pouch cell achieved by using multiple electrolyte additives. J Power Sources 407:173–179. https://doi.org/10.1016/j.jpowsour.2018.08.025
29. Cao X, Zhou HS (2021) An indicator of designing layered sodium-ion oxide materials. Sci Bull 66:753–754. https://doi.org/10.1016/j.scib.2020.12.012
30. Wang Q, Chu S, Guo S (2020) Progress on multiphase layered transition metal oxide cathodes of sodium ion batteries. Chin Chem Lett 31:2167–2176. https://doi.org/10.1016/j.cclet.2019.12.008
31. S. Komaba, N. Yabuuchi, T. Nakayama, A. Ogata, T. Ishikawa, I. Nakai, Study on the reversible electrode reaction of $Na_{1-x}Ni_{0.5}Mn_{0.5}O_2$ for a rechargeable sodium-ion battery, Inorg. Chem. 51 (2012) 6211–6220. https://doi.org/10.1021/ic300357d.
32. S. Komaba, T. Nakayama, A. Ogata, T. Shimizu, C. Takei, S. Takada, A. Hokura, I. Nakai, Electrochemically reversible sodium intercalation of layered $NaNi_{0.5}Mn_{0.5}O_2$ and $NaCrO_2$, ECS Transactions 16 (2009) 43–45. https://doi.org/10.1149/1.3112727.
33. Gao Y, Wang Z, Lu G (2019) Atomistic understanding of structural evolution, ion transport and oxygen stability in layered $NaFeO_2$. J Mater Chem A 7:2619–2625. https://doi.org/10.1039/c8ta10767j
34. Shigeto O, Yusuke T, Toshiyasu K, Takayuki D, Jun-ichi Y, Tetsuaki N (2006) Layered transition metal oxides as cathodes for sodium secondary battery, ECS Meeting Abstracts 02:201. https://doi.org/10.1149/MA2006-02/4/201
35. Mendiboure A, Delmas C, Hagenmuller P (1985) Electrochemical intercalation and deintercalation of $Na_xMnO_2$ bronzes. J Solid State Chem 57:323–331
36. Yu Y, Kong WJ, Li QY, Ning D, Schuck G, Schumacher G, Su CJ, Liu XF (2020) Understanding the multiple effects of $TiO_2$ coating on $NaMn_{0.33}Fe_{0.33}Ni_{0.33}O_2$ cathode material for Na-Ion batteries, ACS Appl. Energy Mater. 3:933–942. https://doi.org/10.1021/acsaem.9b02021.
37. Yabuuchi N, Kajiyama M, Iwatate J, Nishikawa H, Hitomi S, Okuyama R, Usui R, Yamada Y, Komaba S (2012) P2-type $Na_x[Fe_{1/2}Mn_{1/2}]O_2$ made from earth-abundant elements for rechargeable Na batteries. Nat Mater 11:512–517. https://doi.org/10.1038/nmat3309
38. Wang JE, Han WH, Chang KJ, Jung YH, Kim DK (2018) New insight into Na intercalation with Li substitution on alkali site and high performance of O3-type layered cathode material for sodium ion batteries. J Mater Chem A 6:22731–22740. https://doi.org/10.1039/c8ta06159a
39. Birgisson S, Christiansen TL, Iversen BB (2018) Exploration of phase compositions, crystal structures, and electrochemical properties of $Na_xFe_yMn_{1-y}O_2$ sodium ion battery materials. Chem Mater 30:6636–6645. https://doi.org/10.1021/acs.chemmater.8b01566
40. Qi X, Liu L, Song N, Gao F, Yang K, Lu Y, Yang H, Hu YS, Cheng ZH, Chen L (2017) Design and comparative study of O3/P2 hybrid structures for room temperature sodium-ion batteries. ACS Appl Mater Interfaces 9:40215–40223. https://doi.org/10.1021/acsami.7b11282
41. F.X. Ding, C.L. Zhao, D. Zhou, Q.S. Meng, D.D. Xiao, Q.Q. Zhang, Y.S. Niu, Y.Q. Li, X.H. Rong, Y.X. Lu, L.Q. Chen, Y.S. Hu, A novel Ni-rich O3-$Na[Ni_{0.60}Fe_{0.25}Mn_{0.15}]O_2$ cathode for Na-ion batteries, Energy Storage Mater 30 (2020) 420–430. https://doi.org/10.1016/j.ensm.2020.05.013.
42. S.M. Oh, S.T. Myung, C.S. Yoon, J. Lu, J. Hassoun, B. Scrosati, K. Amine, Y.K. Sun, Advanced $Na[Ni_{0.25}Fe_{0.5}Mn_{0.25}]O_2$/C-$Fe_3O_4$ sodium-ion batteries using EMS electrolyte for energy storage, Nano Lett. 14 (2014) 1620–1626. https://doi.org/10.1021/nl500077v.
43. Lamb J, Manthiram A (2020) Synthesis control of layered oxide cathodes for sodium-ion batteries: a necessary step toward practicality. Chem Mater 32:8431–8441. https://doi.org/10.1021/acs.chemmater.0c02435
44. S. Zhao, Q. Shi, R. Qi, X. Zou, $NaTi_2(PO_4)_3$ modified O3-type $NaNi_{1/3}Fe_{1/3}Mn_{1/3}O_2$ as high rate and air stable cathode for sodium-ion batteries, Electrochim. Acta 441 (2023) 141859. https://doi.org/10.1016/j.electacta.2023.141859.
45. H.H. Sun, J.Y. Hwang, C.S. Yoon, A. Heller, C.B. Mullins, Capacity degradation mechanism and cycling stability enhancement of $AlF_3$-coated nanorod gradient $Na[Ni_{0.65}Co_{0.08}Mn_{0.27}]O_2$ cathode for sodium-ion batteries, ACS Nano 12 (2018) 12912–12922. https://doi.org/10.1021/acsnano.8b08266.
46. Yabuuchi N, Kubota K, Dahbi M, Komaba S (2014) Research development on sodium-ion batteries. Chem Rev 114:11636–11682. https://doi.org/10.1021/cr500192f
47. Recent advances in titanium-based electrode materials for stationary sodium-ion batteries, Energy Environ. Sci 9 (2016) 2978–3006. https://doi.org/10.1039/c6ee01807f.
48. Yabuuchi N, Yoshida H, Komaba S (2012) Crystal structures and electrode performance of Alpha-$NaFeO_2$ for rechargeable sodium batteries. Electrochemistry 80:716–719. https://doi.org/10.5796/electrochemistry.80.716
49. Xu J, Han Z, Jiang K, Bai P, Liang Y, Zhang X, Wang P, Guo S, Zhou H (2020) Suppressing cation migration and reducing particle cracks in a layered Fe-based cathode for advanced sodium-Ion batteries. Small 16:1904388. https://doi.org/10.1002/smll.201904388
50. Zhuang Y, Zhao J, Zhao Y, Zhu X, Xia H (2021) Carbon-coated single crystal O3-$NaFeO_2$ nanoflakes prepared via topochemical reaction for sodium-ion batteries. Sustain Mater Technol 28:00258. https://doi.org/10.1016/j.susmat.2021.e00258
51. Ma X, Chen H, Ceder G (2011) Electrochemical Properties of Monoclinic $NaMnO_2$. J Electrochem Soc 158:A1307–A1312. https://doi.org/10.1149/2.035112jes
52. Ma Z, Zhao Z, Xu H, Sun J, He X, Lei Z, Liu ZH, Jiang R, Li Q (2021) A queue-ordered layered Mn-based oxides with Al substitution as high-rate and high-stabilized cathode for sodium-Ion batteries. Small 17:2006259. https://doi.org/10.1002/smll.202006259
53. Zhang X, Qiao Y, Guo S, Jiang K, Xu S, Xu H, Wang P, He P, Zhou H (2019) Manganese-based Na-Rich materials boost anionic redox in high-performance layered cathodes for sodium-ion batteries. Adv Mater 31:1807770. https://doi.org/10.1002/adma.201807770
54. Deng JQ, Luo WB, Lu X, Yao QR, Wang ZM, Liu HK, Zhou HY, Dou SX (2018) High energy density sodium-ion battery with industrially feasible and air-stable O3-type layered oxide cathode. Adv Energy Mater 8:1701610. https://doi.org/10.1002/aenm.201701610
55. Vassilaras P, Ma X, Li X, Ceder G (2012) Electrochemical Properties of Monoclinic $NaNiO_2$. J Electrochem Soc 160:A207–A211. https://doi.org/10.1149/2.023302jes
56. L. Yu, X.-X. Xing, S.-Y. Zhang, X. Zhang, X. Han, P.-F. Wang, S. Xu, Cation-disordered O3-$Na_{0.8}Ni_{0.6}Sb_{0.4}O_2$ cathode for high-voltage sodium-ion batteries, ACS Applied Materials & Interfaces 13 (2021) 32948–32956. https://doi.org/10.1021/acsami.1c06576.
57. P.F. Wang, H. Xin, T.T. Zuo, Q. Li, X. Yang, Y.X. Yin, X. Gao, X. Yu, Y.G. Guo, An abnormal 3.7 Volt O3-type sodium-ion battery cathode, Angew. Chem. Int. Ed. Engl. 57 (2018) 8178–8183. https://doi.org/10.1002/anie.201804130.

58. H. Yu, S. Guo, Y. Zhu, M. Ishida, H. Zhou, Novel titanium-based O3-type $NaTi_{0.5}Ni_{0.5}O_2$ as a cathode material for sodium ion batteries, Chem. Commun. 50 (2014) 457–459. https://doi.org/10.1039/c3cc47351a.
59. Guo S, Sun Y, Liu P, Yi J, He P, Zhang X, Zhu Y, Senga R, Suenaga K, Chen M, Zhou H (2018) Cation-mixing stabilized layered oxide cathodes for sodium-ion batteries. Sci Bull 63:376–384. https://doi.org/10.1016/j.scib.2018.02.012
60. Jiang KZ, Guo SH, Pang WK, Zhang XP, Fang TC, Wang SF, Wang FW, Zhang XY, He P, Zhou HS (2021) Oxygen vacancy promising highly reversible phase transition in layered cathodes for sodium-ion batteries. Nano Res 14:4100–4106. https://doi.org/10.1007/s12274-021-3349-4
61. Li Q, Xu S, Guo S, Jiang K, Li X, Jia M, Wang P, Zhou H (2020) A superlattice-stabilized layered oxide cathode for sodium-ion batteries. Adv Mater 32:1907936. https://doi.org/10.1002/adma.201907936
62. Yuan D, Liang X, Wu L, Cao Y, Ai X, Feng J, Yang H (2014) A honeycomb-layered $Na_3Ni_2SbO_6$: a high-rate and cycle-stable cathode for sodium-ion batteries. Adv Mater 26:6301–6306. https://doi.org/10.1002/adma.201401946
63. P.F. Wang, H.R. Yao, X.Y. Liu, J.N. Zhang, L. Gu, X.Q. Yu, Y.X. Yin, Y.G. Guo, Ti-substituted $NaNi_{0.5}Mn_{0.5-x}Ti_xO_2$ cathodes with reversible O3-P3 phase transition for high-performance sodium-ion batteries, Adv. Mater. 29 (2017) 1700210. https://doi.org/10.1002/adma.201700210.
64. X. Meng, D. Zhang, Z. Zhao, Y. Li, S. Xu, L. Chen, X. Wang, S. Liu, Y. Wu, O3-$NaNi_{0.47}Zn_{0.03}Mn_{0.5}O_2$ cathode material for durable Na-ion batteries, J. Alloys Compd. 887 (2021) 161366. https://doi.org/10.1016/j.jallcom.2021.161366.
65. Sathiya M, Jacquet Q, Doublet M-L, Karakulina OM, Hadermann J, Tarascon J-M (2018) A chemical approach to raise cell voltage and suppress phase transition in O3 sodium layered oxide electrodes. Adv Energy Mater 8:1702599. https://doi.org/10.1002/aenm.201702599
66. J.Y. Hwang, T.Y. Yu, Y.K. Sun, Simultaneous MgO coating and Mg doping of $Na[Ni_{0.5}Mn_{0.5}]O_2$ cathode: facile and customizable approach to high-voltage sodium-ion batteries, J. Mater. Chem. A 6 (2018) 16854–16862. https://doi.org/10.1039/c8ta06551a.
67. D.D. Yuan, Y.X. Wang, Y.L. Cao, X.P. Ai, H.X. Yang, Improved electrochemical performance of Fe-substituted $NaNi_{0.5}Mn_{0.5}O_2$ cathode materials for sodium-ion batteries, ACS Appl. Mater. Interfaces 7 (2015) 8585–8591. https://doi.org/10.1021/acsami.5b00594.
68. Yao HR, Lv WJ, Yin YX, Ye H, Wu XW, Wang Y, Gong Y, Li Q, Yu X, Gu L, Huang Z, Guo YG (2019) Suppression of monoclinic phase transitions of O3-Type cathodes based on electronic delocalization for Na-Ion batteries. ACS Appl Mater Interfaces 11:22067–22073. https://doi.org/10.1021/acsami.9b00186
69. X. Sun, Y. Jin, C.Y. Zhang, J.W. Wen, Y. Shao, Y. Zang, C.H. Chen, $Na[Ni_{0.4}Fe_{0.2}Mn_{0.4-x}Ti_x]O_2$: a cathode of high capacity and superior cyclability for Na-ion batteries, J. Mater. Chem. A 2 (2014) 17268–17271. https://doi.org/10.1039/c4ta03828b.
70. You Y, Xin S, Asl HY, Li W, Wang P-F, Guo Y-G, Manthiram A (2018) Insights into the improved high-voltage performance of Li-incorporated layered oxide cathodes for sodium-Ion batteries. Chem 4:2124–2139. https://doi.org/10.1016/j.chempr.2018.05.018
71. Zhang Q, Huang YY, Liu Y, Sun SX, Wang K, Li YY, Li X, Han JT, Huang YH (2017) F-doped O3-$NaNi_{1/3}Fe_{1/3}Mn_{1/3}O_2$ as high-performance cathode materials for sodium-ion batteries. Sci China Mater 60:629–636. https://doi.org/10.1007/s40843-017-9045-9
72. Ding F, Zhao C, Xiao D, Rong X, Wang H, Li Y, Yang Y, Lu Y, Hu YS (2022) Using high-entropy configuration strategy to design Na-Ion layered oxide cathodes with superior electrochemical performance and thermal stability. J Am Chem Soc 144:8286–8295. https://doi.org/10.1021/jacs.2c02353
73. H. Guo, M. Avdeev, K. Sun, X. Ma, H. Wang, Y. Hu, D. Chen, Pentanary transition-metals Na-ion layered oxide cathode with highly reversible O3-P3 phase transition, Chem. Eng. J. 412 (2021) 128704. https://doi.org/10.1016/j.cej.2021.128704.
74. Li N, Ren J, Dang RB, Wu K, Lee YL, Hu ZB, Xiao XL (2019) Suppressing phase transition and improving electrochemical performances of O3-$NaNi_{1/3}Mn_{1/3}Fe_{1/3}O_2$ through ionic conductive $Na_2SiO_3$ coating. J Power Sources 429:38–45. https://doi.org/10.1016/j.jpowsour.2019.04.052
75. Yu Y, Ning D, Li QY, Franz A, Zheng LR, Zhang N, Ren GX, Schumacher G, Liu XF (2021) Revealing the anionic redox chemistry in O3-type layered oxide cathode for sodium-ion batteries. Energy Storage Mater 38:130–140. https://doi.org/10.1016/j.ensm.2021.03.004
76. Liang X, Sun YK (2022) A novel pentanary metal oxide cathode with P2/O3 biphasic structure for high-performance sodium-Ion batteries. Adv Funct Mater 32:2206154. https://doi.org/10.1002/adfm.202206154
77. Li Y, Gao Y, Wang X, Shen X, Kong Q, Yu R, Lu G, Wang Z, Chen L (2018) Iron migration and oxygen oxidation during sodium extraction from $NaFeO_2$. Nano Energy 47:519–526. https://doi.org/10.1016/j.nanoen.2018.03.007
78. Susanto D, Cho MK, Ali G, Kim J-Y, Chang HJ, Kim H-S, Nam K-W, Chung KY (2019) Anionic redox activity as a key factor in the performance degradation of $NaFeO_2$ cathodes for sodium ion batteries. Chem Mater 31:3644–3651. https://doi.org/10.1021/acs.chemmater.9b00149
79. Lee E, Brown DE, Alp EE, Ren Y, Lu J, Woo J-J, Johnson CS (2015) New insights into the performance degradation of Fe-based layered oxides in sodium-ion batteries: instability of $Fe^{3+}/Fe^{4+}$ redox in α-$NaFeO_2$. Chem Mater 27:6755–6764. https://doi.org/10.1021/acs.chemmater.5b02918
80. Takeda Y, Akagi J, Edagawa A, Inagaki M, Naka S (1980) A preparation and polymorphic relations of sodium iron oxide ($NaFeO_2$). Mat Res Bull 15:1167–1172
81. Kataoka R, Kuratani K, Kitta M, Takeichi N, Kiyobayashi T, Tabuchi M (2015) Influence of the preparation methods on the electrochemical properties and structural changes of alpha-sodium iron oxide as a positive electrode material for rechargeable sodium batteries. Electrochim Acta 182:871–877. https://doi.org/10.1016/j.electacta.2015.09.092
82. Tabuchi M, Kataoka R (2019) Structure and electrochemical properties of α-$NaFeO_2$ obtained under various hydrothermal conditions. J Electrochem Soc 166:A2209–A2214. https://doi.org/10.1149/2.1411910jes
83. Zhao J, Zhao L, Dimov N, Okada S, Nishida T (2013) Electrochemical and thermal properties of α-$NaFeO_2$ cathode for Na-Ion batteries. J Electrochem Soc 160:A3077–A3081. https://doi.org/10.1149/2.007305jes
84. Yan P, Zheng J, Chen T, Luo L, Jiang Y, Wang K, Sui M, Zhang JG, Zhang S, Wang C (2018) Coupling of electrochemically triggered thermal and mechanical effects to aggravate failure in a layered cathode. Nat Commun 9:2437. https://doi.org/10.1038/s41467-018-04862-w
85. J. Jayachitra, A. Balamurugan, J. Richards Joshua, V. Sharmila, N. Sivakumar, T. Alshahrani, M. Shkir, Enhancing the electrochemical performance by structural evolution in O3- $NaFe_{1-x}Mg_xO_2$ cathodes for sodium ion batteries, Inorg. Chem. Commun. 129 (2021) 108528. https://doi.org/10.1016/j.inoche.2021.108528.
86. Liu L, Li X, Bo S-H, Wang Y, Chen H, Twu N, Wu D, Ceder G (2015) High-performance P2-Type $Na_{2/3}(Mn_{1/2}Fe_{1/4}Co_{1/4})O_2$ cathode material with superior rate capability for Na-Ion batteries. Adv Energy Mater 5:1500944. https://doi.org/10.1002/aenm.201500944
87. H.-R. Yao, W.-J. Lv, X.-G. Yuan, Y.-J. Guo, L. Zheng, X.-A. Yang, J. Li, Y. Huang, Z. Huang, P.-F. Wang, Y.-G. Guo, New insights to build $Na^+$/vacancy disordering for high-performance P2-type layered oxide cathodes, Nano Energy 97 (2022) 107207. https://doi.org/10.1016/j.nanoen.2022.107207.
88. Wang X, Liu G, Iwao T, Okubo M, Yamada A (2014) Role of ligand-to-metal charge transfer in O3-Type $NaFeO_2$–$NaNiO_2$ solid solution for enhanced electrochemical properties. J PHYS CHEM C 118:2970–2976. https://doi.org/10.1021/jp411382r
89. I. Moeez, D. Susanto, G. Ali, H.-G. Jung, H.-D. Lim, K.Y. Chung, Effect of the interfacial protective layer on the $NaFe_{0.5}Ni_{0.5}O_2$ cathode for rechargeable sodium-ion batteries, J. Mater. Chem. A 8 (2020) 13964–13970. https://doi.org/10.1039/d0ta02837a.
90. J.S. Thorne, S. Chowdhury, R.A. Dunlap, M.N. Obrovac, Structure and electrochemistry of $Na_xFe_xTi_{1-x}O_2$($1.0 \geq x \geq 0.75$) for Na-Ion battery positive electrodes, J. Electrochem. Soc. 161 (2014) A1801-A1805. https://doi.org/10.1149/2.0291412jes.
91. J. Molenda, A. Plewa, A. Kulka, Ł. Kondracki, K. Walczak, A. Milewska, M. Rybski, L. Lu, J. Tobola, The effect of O3–P3–P′3 phases coexistence in $Na_xFe_{0.3}Co_{0.7}O_2$ cathode material on its electronic and electrochemical properties. Experimental and theoretical studies, J. Power Sources 449 (2020) 227471. https://doi.org/10.1016/j.jpowsour.2019.227471.
92. H. Yoshida, N. Yabuuchi, S. Komaba, $NaFe_{0.5}Co_{0.5}O_2$ as high energy and power positive electrode for Na-ion batteries, Electrochem. Commun. 34 (2013) 60–63. https://doi.org/10.1016/j.elecom.2013.05.012.

93. Parant J-P, Olzacuaga R, Devalette M (1971) Sur quelques nouvelles phases de formule $Na_xMnO_2$ (x ⩽ 1). J Solid State Chem 3:1–11
94. Chen M, Liu Q, Wang SW, Wang E, Guo X, Chou SL (2019) High-abundance and low-cost metal-based cathode materials for sodium-ion batteries: problems, progress, and key technologies. Adv Energy Mater 9:1803609. https://doi.org/10.1002/aenm.201803609
95. Abakumov AM, Tsirlin AA, Bakaimi I, Van Tendeloo G, Lappas A (2014) Multiple twinning as a structure directing mechanism in layered rock-salt-type oxides: $NaMnO_2$ polymorphism, redox potentials, and magnetism. Chem Mater 26:3306–3315. https://doi.org/10.1021/cm5011696
96. Billaud J, Clement RJ, Armstrong AR, Canales-Vazquez J, Rozier P, Grey CP, Bruce PG (2014) β-$NaMnO_2$: a high-performance cathode for sodium-ion batteries. J Am Chem Soc 136:17243–17248. https://doi.org/10.1021/ja509704t
97. Clément RJ, Middlemiss DS, Seymour ID, Ilott AJ, Grey CP (2016) Insights into the nature and evolution upon electrochemical cycling of planar defects in the β-$NaMnO_2$ Na-Ion battery cathode: an NMR and first-principles density functional theory spproach. Chem Mater 28:8228–8239. https://doi.org/10.1021/acs.chemmater.6b03074
98. Velikokhatnyi OI, Chang CC, Kumta PN (2003) Phase stability and electronic structure of $NaMnO_2$. J Electrochem Soc 150:A1262–A1266. https://doi.org/10.1149/1.1600464
99. Kumakura S, Tahara Y, Kubota K, Chihara K, Komaba S (2016) Sodium and manganese stoichiometry of P2-Type $Na_{2/3}MnO_2$. Angew Chem Int Ed Engl 55:12760–12763. https://doi.org/10.1002/anie.201606415
100. J. Lamb, A. Manthiram, Surface-modified $Na(Ni_{0.3}Fe_{0.4}Mn_{0.3})O_2$ cathodes with enhanced cycle life and air stability for sodium-ion batteries, ACS Appl. Energy Mater. 4 (2021) 11735–11742. https://doi.org/10.1021/acsaem.1c02485.
101. Kim D, Cho M, Cho K (2017) Rational design of Na(Li1/3Mn2/3)O2 operated by anionic redox reactions for advanced sodium-Ion batteries. Adv Mater 29:1701788. https://doi.org/10.1002/adma.201701788
102. Y. Zhang, J. Wang, L. Wang, L. Duan, G. Zhang, F. Zhao, X. Zhang, W. Lü, The multi-metal synergetic mechanism of O3-$Na_{0.5}Mn_{0.65}Ni_{0.15}Al_{0.1}Mg_{0.05}Co_{0.05}O_2$ nanoflower for a high-voltage and long-cycle-life cathode material of sodium-ion batteries, Journal of Materials Science 55 (2020) 13102–13113. https://doi.org/10.1007/s10853-020-04940-9.
103. Braconnier JJ, Delmas C, Hagenmuller P (1982) Etude par Desintercalation electrochimique des systemes $NaxCrO_2$ et NaxNiO2[J]. Mater Res Bull 17:993–1000. https://doi.org/10.1016/0025-5408(82)90124-6
104. Delmas C, Borthomieu Y, Faure C, et al (1989) Nickel hydroxide and derived phases obtained by chimie douce from $NaNiO_2$. Solid State Ionics 32-33:104–111. https://doi.org/10.1016/0167-2738(88)90073-2
105. Molenda J, StokŁosa A (1990) Electronic and electrochemical properties of nickel bronze, $NaxNiO_2$. Solid State Ionics 38(1–2):1–4. https://doi.org/10.1016/0167-2738(90)90438-W
106. Han MH, Gonzalo E, Casas-Cabanas M, Rojo T (2014) Structural evolution and electrochemistry of monoclinic $NaNiO_2$ upon the first cycling process. J Power Sources 258:266–271. https://doi.org/10.1016/j.jpowsour.2014.02.048
107. Wang L, Wang J, Zhang X, Ren Y, Zuo P, Yin G, Wang J (2017) Unravelling the origin of irreversible capacity loss in $NaNiO_2$ for high voltage sodium ion batteries. Nano Energy 34:215–223. https://doi.org/10.1016/j.nanoen.2017.02.046
108. J. Han, Y. Niu, Y. Zhang, J. Jiang, S.-j. Bao, M. Xu, Evaluation of O3-type $Na_{0.8}Ni_{0.6}Sb_{0.4}O_2$ as cathode materials for sodium-ion batteries, J. Solid State Electrochem. 20 (2016) 2331–2335. https://doi.org/10.1007/s10008-016-3255-y.
109. C. Delmas, I. Saadoune, P. Dordor, Effect of cobalt substitution on the Jahn-Teller distortion of the $NaNiO_2$ layered oxide, Molecular Crystals and Liquid Crystals Science and Technology. Section A. Molecular Crystals and Liquid Crystals 244 (1994) 337–342. https://doi.org/10.1080/10587259408050127.
110. Saadoune I, Maazaz A, Ménétrier M, Delmas C (1996) On the $NaxNi_{0.6}Co_{0.4}O_2$ System: Physical and Electrochemical Studies. J Solid State Chem 122;111-117. https://doi.org/10.1006/jssc.1996.0090
111. Vassilaras P, Kwon D-H, Dacek ST, Shi T, Seo D-H, Ceder G, Kim JC (2017) Electrochemical properties and structural evolution of O3-type layered sodium mixed transition metal oxides with trivalent nickel. J Mater Chem A 5:4596–4606. https://doi.org/10.1039/c6ta09220a
112. X. Rong, X. Qi, Y. Lu, Y. Wang, Y. Li, L. Jiang, K. Yang, F. Gao, X. Huang, L. Chen, Y.-S. Hu, A new Tin-based O3-$Na_{0.9}[Ni_{0.45-x/2}Mn_xSn_{0.55-x/2}]O_2$ as sodium-ion battery cathode, J Energy Chem 31 (2019) 132–137. https://doi.org/10.1016/j.jechem.2018.05.019.
113. S. Maletti, A. Sarapulova, A. Schokel, D. Mikhailova, Operando studies on the $NaNi_{0.5}Ti_{0.5}O_2$ cathode for Na-Ion batteries: elucidating titanium as a structure stabilizer, ACS Appl. Mater. Interfaces 11 (2019) 33923–33930. https://doi.org/10.1021/acsami.9b10352.
114. Seibel EM, Roudebush JH, Wu H, Huang Q, Ali MN, Ji H, Cava RJ (2013) Structure and magnetic properties of the alpha-$NaFeO_2$-type honeycomb compound $Na_3Ni_2BiO_6$. Inorg Chem 52:13605–13611. https://doi.org/10.1021/ic402131e
115. Bhange DS, Ali G, Kim D-H, Anang DA, Shin TJ, Kim M-G, Kang Y-M, Chung KY, Nam K-W (2017) Honeycomb-layer structured $Na_3Ni_2BiO_6$ as a high voltage and long life cathode material for sodium-ion batteries. J Mater Chem A 5:1300–1310. https://doi.org/10.1039/c6ta08661f
116. Schmidt W, Berthelot R, Sleight AW, Subramanian MA (2013) Solid solution studies of layered honeycomb-ordered phases O3–$Na_3M_2SbO_6$ (M=Cu, Mg, Ni, Zn). J Solid State Chem 201:178–185. https://doi.org/10.1016/j.jssc.2013.02.035
117. Wang PF, Weng M, Xiao Y, Hu Z, Li Q, Li M, Wang YD, Chen X, Yang X, Wen Y, Yin YX, Yu X, Xiao Y, Zheng J, Wan LJ, Pan F, Guo YG (2019) An ordered $Ni_6$-ring superstructure enables a highly stable sodium oxide cathode. Adv Mater 31:1903483. https://doi.org/10.1002/adma.201903483
118. de la Llave E, Borgel V, Park KJ, Hwang JY, Sun YK, Hartmann P, Chesneau FF, Aurbach D (2016) Comparison between Na-Ion and Li-Ion cells: understanding the critical role of the cathodes stability and the anodes pretreatment on the cells behavior. ACS Appl Mater Interfaces 8:1867–1875. https://doi.org/10.1021/acsami.5b09835
119. Komaba S, Murata W, Ishikawa T, Yabuuchi N, Ozeki T, Nakayama T, Ogata A, Gotoh K, Fujiwara K (2011) Electrochemical Na insertion and solid electrolyte interphase for hard-carbon electrodes and application to Na-Ion batteries. Adv Funct Mater 21:3859–3867. https://doi.org/10.1002/adfm.201100854
120. Komaba S, Ishikawa T, Yabuuchi N, Murata W, Ito A, Ohsawa Y (2011) Fluorinated ethylene carbonate as electrolyte additive for rechargeable Na batteries. ACS Appl Mater Interfaces 3:4165–4168. https://doi.org/10.1021/am200973k
121. Oh SM, Myung ST, Jang MW, Scrosati B, Hassoun J, Sun YK (2013) An advanced sodium-ion rechargeable battery based on a tin-carbon anode and a layered oxide framework cathode. Phys Chem Chem Phys 15:3827–3833. https://doi.org/10.1039/c3cp00070b
122. Dahn ZLJR (2001) Intercalation of water in P2, T2 and O2 structure $A_z[Co_xNi_{1/3-x}Mn_{2/3}]O_2$. Chem Mater 13:1252–1257. https://doi.org/10.1021/cm000721x
123. Air-stability of sodium-based layered-oxide cathode materials (2022) SCIENCE CHINA Chem 65:1076–1087. https://doi.org/10.1007/s11426-022-1257-8
124. Zhang Y, Zhang R, Huang Y (2019) Air-stable $Na_xTMO_2$ cathodes for sodium storage. Front Chem 7:335. https://doi.org/10.3389/fchem.2019.00335
125. You Y, Dolocan A, Li W, Manthiram A (2019) Understanding the air-exposure degradation chemistry at a nanoscale of layered oxide cathodes for sodium-Ion batteries. Nano Lett 19:182–188. https://doi.org/10.1021/acs.nanolett.8b03637
126. Zhao S, Shi Q, Feng W, Liu Y, Yang X, Zou X, Lu X, Zhao Y (2023) Suppression of multistep phase transitions of O3-type cathode for sodium-ion batteries. Chin Chem Lett. https://doi.org/10.1016/j.cclet.2023.108606
127. Kubota K, Fujitani N, Yoda Y, Kuroki K, Tokita Y, Komaba S (2021) Impact of Mg and Ti doping in O3 type $NaNi_{1/2}Mn_{1/2}O_2$ on reversibility and phase transition during electrochemical Na intercalation. J Mater Chem A 9:12830–12844. https://doi.org/10.1039/d1ta01164b
128. N.Y. Hong, K. Wu, Z.J. Peng, Z.H. Zhu, G.F. Jia, M. Wang, Improved high rate performance and cycle performance of Al-doped O3-type $NaNi_{0.5}Mn_{0.5}O_2$ cathode materials for sodium-Ion batteries, J Phys Chem C 124 (2020) 22925–22933. https://doi.org/10.1021/acs.jpcc.0c06032.
129. Q. Zhang, Q.F. Gu, Y. Li, H.N. Fan, W.B. Luo, H.K. Liu, S.X. Dou, Surface stabilization of O3-type layered oxide cathode to protect the anode of sodium ion batteries for superior lifespan, iScience 19 (2019) 244–254. https://doi.org/10.1016/j.isci.2019.07.029.

130. Ahmed B, Xia C, Alshareef HN (2016) Electrode surface engineering by atomic layer deposition: A promising pathway toward better energy storage. Nano Today 11:250–271. https://doi.org/10.1016/j.nantod.2016.04.004
131. Yu F, Du L, Zhang G, Su F, Wang W, Sun S (2019) Electrode engineering by atomic layer deposition for sodium-ion batteries: from traditional to advanced batteries. Adv Funct Mater 30:1906890. https://doi.org/10.1002/adfm.201906890
132. Meng X, Wang X, Geng D, Ozgit-Akgun C, Schneider N, Elam JW (2017) Atomic layer deposition for nanomaterial synthesis and functionalization in energy technology. Mater Horiz 4:133–154. https://doi.org/10.1039/c6mh00521g
133. L.Y. Yang, S.W. Sun, K. Du, H.L. Zhao, D. Yan, H.Y. Yang, C.Y. Yu, Y. Bai, Prompting structure stability of O3–$NaNi_{0.5}Mn_{0.5}O_2$ via effective surface regulation based on atomic layer deposition, Ceram. Int. 47 (2021) 28521–28527. https://doi.org/10.1016/j.ceramint.2021.07.009.
134. Y. Xiao, T. Wang, Y.F. Zhu, H.Y. Hu, S.J. Tan, S. Li, P.F. Wang, W. Zhang, Y.B. Niu, E.H. Wang, Y.J. Guo, X. Yang, L. Liu, Y.M. Liu, H. Li, X.D. Guo, Y.X. Yin, Y.G. Guo, Large-scale synthesis of the stable co-free layered oxide cathode by the synergetic contribution of multielement chemical substitution for practical sodium-Ion battery, Research (2020) 1469301. https://doi.org/10.34133/2020/1469301.
135. Kubota K, Komaba S (2015) Review—practical issues and future perspective for Na-Ion batteries. J Electrochem Soc 162:A2538–A2550. https://doi.org/10.1149/2.0151514jes
136. L. Zheng, L. Li, R. Shunmugasundaram, M.N. Obrovac, Effect of controlled-atmosphere storage and ethanol rinsing on $NaNi_{0.5}Mn_{0.5}O_2$ for sodium-Ion batteries, ACS Appl. Mater. Interfaces 10 (2018) 38246–38254. https://doi.org/10.1021/acsami.8b14209.
137. Hwang J-Y, Myung S-T, Aurbach D, Sun Y-K (2016) Effect of nickel and iron on structural and electrochemical properties of O3 type layer cathode materials for sodium-ion batteries. J Power Sources 324:106–112. https://doi.org/10.1016/j.jpowsour.2016.05.064
138. H. Zhao, J.Z. Li, W.P. Liu, H.Y. Xu, X.W. Gao, J.J. Shi, K. Yu, X.Y. Ding, Integrated titanium-substituted air stable O3 sodium layered oxide electrode via a complexant assisted route for high capacity sodium-ion battery, Electrochim. Acta 388 (2021) 138561. https://doi.org/10.1016/j.electacta.2021.138561.
139. Hwang T, Lee JH, Choi SH, Oh RG, Kim D, Cho M, Cho W, Park MS (2019) Critical role of titanium in O3-type layered cathode materials for sodium-ion batteries. ACS Appl Mater Interfaces 11:30894–30901. https://doi.org/10.1021/acsami.9b08987
140. S.-M. Oh, S.-T. Myung, J.-Y. Hwang, B. Scrosati, K. Amine, Y.-K. Sun, High capacity O3-Type $Na[Li_{0.05}(Ni_{0.25}Fe_{0.25}Mn_{0.5})_{0.95}]O_2$ cathode for sodium ion batteries, Chem. Mater. 26 (2014) 6165–6171. https://doi.org/10.1021/cm502481b.
141. C. Zhang, R. Gao, L. Zheng, Y. Hao, X. Liu, New insights into the roles of Mg in improving the rate capability and cycling stability of O3-$NaMn_{0.48}Ni_{0.2}Fe_{0.3}Mg_{0.02}O_2$ for sodium-ion batteries, ACS Appl. Mater. Interfaces 10 (2018) 10819–10827. https://doi.org/10.1021/acsami.7b18226.
142. Sun L, Xie Y, Liao XZ, Wang H, Tan G, Chen Z, Ren Y, Gim J, Tang W, He YS, Amine K, Ma ZF (2018) Insight into Ca-substitution effects on O3-type $NaNi_{1/3}Fe_{1/3}Mn_{1/3}O_2$ cathode materials for sodium-ion batteries application. Small 14:1704523. https://doi.org/10.1002/smll.201704523
143. Ma A, Yin Z, Wang J, Wang Z, Guo H, Yan G (2020) Al-doped $NaNi_{1/3}Mn_{1/3}Fe_{1/3}O_2$ for high performance of sodium ion batteries. Lonics 26:1797–1804. https://doi.org/10.1007/s11581-019-03437-z
144. Q. Mao, C. Zhang, W. Yang, J. Yang, L. Sun, Y. Hao, X. Liu, Mitigating the voltage fading and lattice cell variations of O3-$NaNi_{0.2}Fe_{0.35}Mn_{0.45}O_2$ for high performance Na-ion battery cathode by Zn doping, J. Alloys Compd. 794 (2019) 509–517. https://doi.org/10.1016/j.jallcom.2019.04.271.
145. Sarkar A, Wang Q, Schiele A, Chellali MR, Bhattacharya SS, Wang D, Brezesinski T, Hahn H, Velasco L, Breitung B (2019) High-entropy oxides: fundamental aspects and electrochemical properties. Adv Mater 31:1806236. https://doi.org/10.1002/adma.201806236
146. H. Chen, S. Li, S. Huang, L. Ma, S. Liu, F. Tang, Y. Fang, P. Dai, High-entropy structure design in layered transition metal dichalcogenides, Acta Mater. 222 (2022) 117438. https://doi.org/10.1016/j.actamat.2021.117438.
147. Fu F, Liu X, Fu X, Chen H, Huang L, Fan J, Le J, Wang Q, Yang W, Ren Y, Amine K, Sun SG, Xu GL (2022) Entropy and crystal-facet modulation of P2-type layered cathodes for long-lasting sodium-based batteries. Nat Commun 13:2826. https://doi.org/10.1038/s41467-022-30113-0
148. Lin C-C, Liu H-Y, Kang J-W, Yang C-C, Li C-H, Chen H-YT, Huang S-C, Ni C-S, Chuang Y-C, Chen B-H, Chang C-K, Chen H-Y (2022) In-situ X-ray studies of high-entropy layered oxide cathode for sodium-ion batteries. Energy Storage Mater 51:159–171. https://doi.org/10.1016/j.ensm.2022.06.035
149. Miracle DB, Senkov ON (2017) A critical review of high entropy alloys and related concepts. Acta Mater 122:448–511. https://doi.org/10.1016/j.actamat.2016.08.081
150. Ma Y, Ma Y, Wang Q, Schweidler S, Botros M, Fu T, Hahn H, Brezesinski T, Breitung B (2021) High-entropy energy materials: challenges and new opportunities. Energy Environ Sci 14:2883–2905. https://doi.org/10.1039/d1ee00505g
151. Q. Deng, F.H. Zheng, W.T. Zhong, Q.Z. Pan, Y.Z. Liu, Y.P. Li, Y.J. Li, J.H. Hu, C.H. Yang, M.L. Liu, Nanoscale surface modification of P2-type $Na_{0.65}[Mn_{0.70}Ni_{0.16}Co_{0.14}]O_2$ cathode material for high-performance sodium-ion batteries, Chem. Eng. J. 404 (2021) 126446. https://doi.org/10.1016/j.cej.2020.126446.
152. J.R. Wang, Q. Zhou, J.Y. Liao, X. Ding, Q. Hu, X.D. He, C.H. Chen, Suppressing the unfavorable surface layer growth on $Na_{0.44}MnO_2$ cathode by a $NaTi_2(PO_4)_3$ coating to improve cycling stability and ultrahigh rate capability, ACS Appl. Energy Mater. 2 (2019) 7497–7503. https://doi.org/10.1021/acsaem.9b01471.
153. Hwang JY, Myung ST, Choi JU, Yoon CS, Yashiro H, Sun YK (2017) Resolving the degradation pathways of the O3-type layered oxide cathode surface through the nano-scale aluminum oxide coating for high-energy density sodium-ion batteries. J Mater Chem A 5:23671–23680. https://doi.org/10.1039/c7ta08443a
154. Keller M, Buchholz D, Passerini S (2016) Layered Na-Ion cathodes with outstanding performance resulting from the synergetic effect of mixed P- and O-Type phases. Adv Energy Mater 6:1501555. https://doi.org/10.1002/aenm.201501555
155. Wang K, Wu Z-G, Melinte G, Yang Z-G, Sarkar A, Hua W, Mu X, Yin Z-W, Li J-T, Guo X-D, Zhong B-H, Kübel C (2021) Preparation of intergrown P/O-type biphasic layered oxides as high-performance cathodes for sodium ion batteries. J Mater Chem A 9:13151–13160. https://doi.org/10.1039/d1ta00627d


## Publisher's Note